universität wien

MASTERARBEIT

Titel der Masterarbeit

„Optical Trapping and Transport of Nanoparticles with Hollow Core Photonic Crystal Fibers“

Verfasser

David Grass, BSc

angestrebter akademischer Grad

Master of Science, MSc

Wien, 2013

Studienkennzahl lt. Studienblatt:	A 066876
Studienrichtung lt. Studienblatt:	Physik
Betreuerin / Betreuer:	Univ.-Prof. Dr. Markus Aspelmeyer

Optical trapped, small spheres in ultra-high vacuum recently gained attention as an opto-mechanical system that allows testing fundamental questions in physics [1, 2, 3, 4, 5]. One of the challenges for those types of experiments is the preparation of a nanometer sized particle in an ultra-high vacuum.

Particle sizes typically proposed for those experiments are around 100nm. The two common approaches to prepare nanoparticles in an optical trap are limited. Shaking particles loose from a piezoelectric crystal is strongly constrained by Van der Waals forces. The approach based on liquid droplets containing nanoparticles is detrimental for the vacuum.

This thesis introduces a novel particle source combining a nebulizer source with optical trapping and a hollow core photonic crystal fiber. The fiber provides a 10μm wide core connecting a nebulizer source with a science chamber. An optical trap is prepared through the hollow core fiber. It provides a transport mechanism capable of trapping a single nanoparticle from the nebulizer source and moving it in a controlled way into the science chamber.

The experiment performed demonstrates the basic working principle by transporting nanoparticles from a nebulizer source through a hollow core photonic crystal fiber into a science chamber at room pressure. The setup allows high positioning accuracy and characterisation of the nanoparticle dynamics. The system is demonstrated to be compatible with an ultra-high vacuum environment and promises transport of nanoparticles into ultra-high vacuum.

Acknowledgements

First I want to thank Markus for giving me the opportunity to work in his research group providing this excellent environment to study physics. One of the main reasons for this are, of course, the group members. Thank you all Garrett, Claus, Simon, Jason, Joachim, Sebastian, Sungkun, Rainer, Philipp, Stephen, Ralf, Jonas, Alex, Karoline, Michael and Witlef for listening to my problems and supporting me all the time. Uros, Florian and Nikolai deserve special thanks as they have to deal with "my stuff" on a daily basis which is not always easy, I assume. Nevertheless you are always helping where you can, which I cannot appreciate enough.

During my Erasmus term in Southampton Hendrik Ulbricht gave me the opportunity to work in his labs, thank you so much for giving me the chance to discover my pleasure in experimental physics, especially as the subject of my thesis is a continuation of our work we started there.

Despite my colleagues there are many friends and co-students I want to express my gratitude and without whom I would not have been able to accomplish my studies. This also goes to the Kaiserslautern people, Jonas, Sören, Malte, Dennis and Fabian. You know why.

Last and most important I thank my family[1] and especially my parents ....the list of things I would like to write is way too long ...they know what they did and so do I. Thank you for everything.

This list is rather incomplete. There are many other people who deserve my acknowledgments but I cannot name all of them. Life would not be as good as without them.

David Grass
Wien, Juli 2013

[1]For me, family does not necessarily imply relative and the other way round, it means people very close to me

Contents

1. Introduction **1**
1.1. Requirements for a Particle Source . . . 1
1.2. A novel Loading Mechanism . . . 3
1.3. Throughput of a hollow core photonic crystal fiber . . . 4

2. Optical Trapping **8**
2.1. Gaussian Beam . . . 8
2.2. Standing Wave . . . 9
2.3. Radiation Forces and Harmonic Potential . . . 9
2.4. Damping . . . 11
2.5. Noise Power Spectrum of a Harmonic Oscillator . . . 13
2.6. Position Detection . . . 14

3. Hollow Core Photonic Crystal Fibers **17**
3.1. Photonic Crystals . . . 17
3.2. Symmetries . . . 19
3.3. Bandgap Diagrams . . . 21
3.4. Properties . . . 22

4. State of the Art **24**
4.1. Leviatation and Guidance of Particles in Air . . . 24
4.2. Trapping of Particles in Liquid filled Hollow Core Photonic Crystal Fiber 26

5. Experiment and Methods **28**
5.1. Experimental Setup . . . 28
5.2. Evaporative Source and Particle Preparation . . . 29
5.3. Optical Trap . . . 30
5.4. Moving Mechanisms . . . 31
5.4.1. Particle Propelling . . . 31
5.4.2. Particle Motion due to an overall Frequency Change . . . 32
5.4.3. Particle Motion due to Displacement of the Standing Wave . . . 33
5.5. Position Read Out . . . 34

6. Disscussion and Results **35**
6.1. Trapping . . . 35
6.2. Particle Transport . . . 36
6.3. Position Readout . . . 37

7. Conclusions and Outlook **40**

A. HC-1060 Data Sheet **42**

B. HCPCF Cleaving **43**

C. Zusammenfassung **45**

D. Curriculm Vitae **46**

List of Figures

1. Required acceleration to break off Van der Waals forces 2
2. String of nanoparticles in a Fabry-Perrot cavity 3
3. Novel loading mechanism for nanoparticles 3
4. Knudsen number for a small tube 5
5. Throughput of a HCPCF and a vacuum pump 6
6. Gradient force on a nanosphere 10
7. Damping rate of a nanoparticle in air 12
8. Spectrum of a harmonic oscillator 14
9. Position readout 15
10. Axial position readout 16
11. Picture of the HC1060 HCPCF from NKTPhotonics 17
12. Photonic crystal fiber 19
13. Bandgap diagramm from [6] 21
14. Bandgap diagramm from [7] 23
15. Benabid et al. experiment [8] 25
16. Schmidt et al. experiment [9] 25
17. Summary of key values of state of the art experiments 26
18. Transverse trapping in HCPCF 26
19. Experimental setup 28
20. Trap depth 31
21. Particle velocity in a HCPCF 32
22. Particle transport by an overall frequency change 33
23. Trapped nanoparticles in front of a HCPCF 35
24. Particle transportation inside a HCPCF 36
25. Particle transport by scattering force 37
26. Particle transport by an overall frequency change 37
27. Noise power spectra of a trapped nanoparticle 38
28. Frequency power measurement of a trapped nanoparticle 39
29. Pressure distribution along a HCPCF 41
30. Three different cleaves with a Fujikura CT-30 43
31. Three different cleaves with a VF-15-H 43
32. Three different cleaves done manually 43

1. Introduction

Quantum mechanics is a well tested theory for the microscopic world describing electrons, atoms and molecules for example. A still open question is if quantum mechanics can also describe macroscopic systems or if the theory breaks down reaching a certain size or mass of objects. The field of cavity optomechanics [10] is a good candidate to reach experimental regimes where this questions can be answered.

In 2010 three proposals for cavity optomechanics with levitated nanospheres were published [1, 2, 3] and another [4] in 2011. The main idea is optically trapping a small dielectric particle (arround 100nm radius) in a Fabry-Perot cavity. The particle behaves as an harmonic oscillator which has a dispersive coupling to the cavity mode. The particle moves along an intensity gradient inside the cavity mode due to the Brownian motion changing the effective cavity length. This mechanism allows control, manipulation and read out of the centre of mass motion of the particle. A big step towards the regime proposed is cooling the centre of mass motion to the quantum mechanical groundstate.

One crucial parameter for cavity optomechanics with levitated nanospheres is the pressure of the environment. An experiment based on those proposals, an experiment we are working on [11], requires a pressure of 10^{-7}mbar to cool to the groundstate of the centre of mass motion. One of the challenges is therefore the development of a vacuum compatible loading mechanism for nanoparticles.

Most experiments dealing with levitating nanospheres use a nebulizer source to load particles in an optical trap. For example a medical asthma spray is used in [12, 13, 11] to nebulize a solution of nanoparticles. Then, trapping is a random process without control where a particle occupies the trap and how many particles are in the trap.

A second aspect of nebulizer sources is contamination of the vacuum chamber. To cool a nanoparticle to the groundstate of its centre of mass motion sufficiently low pressures are required. The level of contamination by loading with nebulizer sources, as they also load solvent, is too high to reach the required vacuum.

Ideally one would be able to prepare one nanoparticle and transfer it to the desired place into an ultrahigh vacuum (UHV) chamber, without contamination and with control over particle number and position.

1.1. Requirements for a Particle Source

The main requirements are having a dry source which is compatible with UHV and being able to prepare nanoparticles of the desired size, 127nm for our levitation experiment [11], at the desired position.

The early experiments by Ashkin [14, 15] showed trapping of a 20μm sphere in a vacuum of 10^{-6}mbar with a piezoelectric loading mechanism. Spheres were prepared on a microscope cover slide attached to a piezoelectric crystal. Driving the piezo with an AC voltage accelerates the particles sufficiently enough to overcome Van der Waals forces that bind the spheres on the glass slide. This source was positioned in such a way that particles leaving the glass slide fell into the optical trap. The Van der Waals force

between a spherical particle and a flat surface is given by [16]

$$F_{\mathrm{VdW}}(z) = \frac{A_{\mathrm{H}} a}{8\pi z^2} \tag{1}$$

with A_{H} the Hamaker constant taking into account the material properties of the sphere and the surface, a the sphere radius and z the distance between the particle and the surface. If a particle is attached on a surface the separation distance is usually assumed to be $z = 4 \times 10^{-10}$m [17, 18, 19]. To estimate the precise adhesive force between a particle and a surface more effects than just Van der Waals force, like particle deformation caused by Van der Waals forces which increase the contact area, surface roughness, etc. have to be taken into account but equation 1 is sufficient to estimate the magnitude.

The piezo attached on the glass slide is driven with a sinusoidal signal and the acceleration acting on a particle sticking on the surface can maximally be $f^2 A$ with A the elongation of the piezo and f the driving frequency. Whenever the force caused by the piezo overcomes the Van der Waals force particles leave the surface. Figure 1 shows an

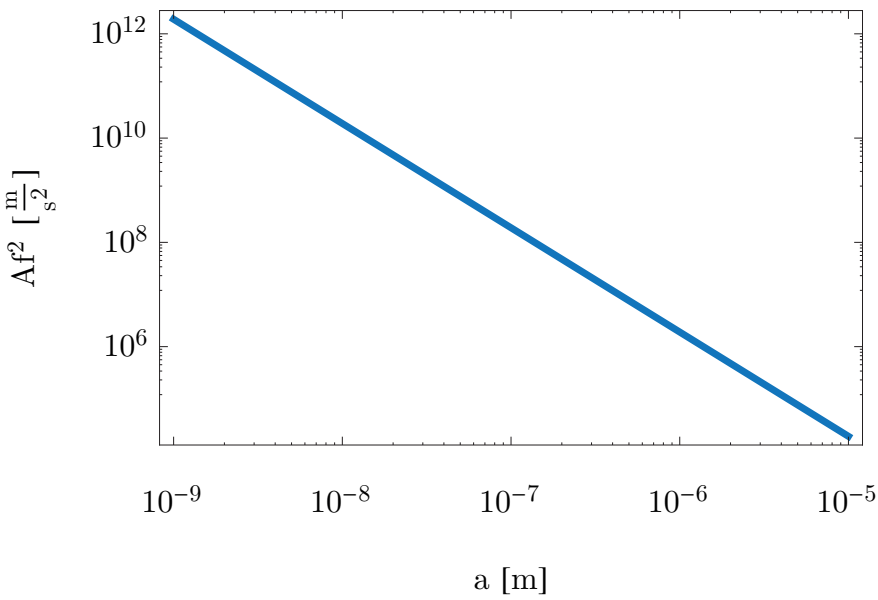

Figure 1: Required acceleration Af^2 to break Van der Waals forces between a silica particle with radius a and a silica cover slide

estimation of the acceleration needed to overcome Van der Waals forces between a silica sphere and a silica cover slide depending on its radius a (Hamaker constant for silica surface an silica particle: $A_{\mathrm{H}} = 8.5 \times 10^{-20}$J, [20]). If one wants to use a piezoelectric source for launching particles of 50nm radius as proposed in [1] or 127nm particles as used in [11] an acceleration of $7 \times 10^7 \frac{\mathrm{m}}{\mathrm{s}^2}$ or $1 \times 10^7 \frac{\mathrm{m}}{\mathrm{s}^2}$ respectively is required. A piezoelectric crystal would need an elongation of 1μm at 1MHz frequency for example which is far out of reach of current state of the art technology. The shaking method is limited

to particles of several micrometers in size and not capable of getting nanometer sized particles loose from a surface. Li et al. used this technique in their experiments and were not able to launch particles with a size smaller than 1μm [21].

The piezoelectric crystal is a dry source allowing the usage in UHV but is limited to micrometer sized particles. Note, however that additional heating of the piezo offers a way to decrease the particle size[22].

Another way of preparing particles is a nebulizer source, as mentioned in the introduction or in more detail in chapter 5.2. A solution of particles is nebulized and then brought to an optical trap. This method is reported to work for sphere radii between 26-510nm [13], but is not UHV compatible because of contamination.

In addition, the particles are randomly moving into the trap and it is unpredictable how many of them occupy the trap. This argument also holds for particles leaving a piezoelectric source.

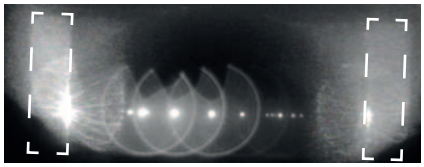

Figure 2: String of nanoparticles trapped inside a Fabry-Perrot cavity (dashed line), loaded with a nebulizer source

Figure 2 gives an example of random occupation of a Fabry-Perrot cavity loaded with a nebulizer source.

1.2. A novel Loading Mechanism

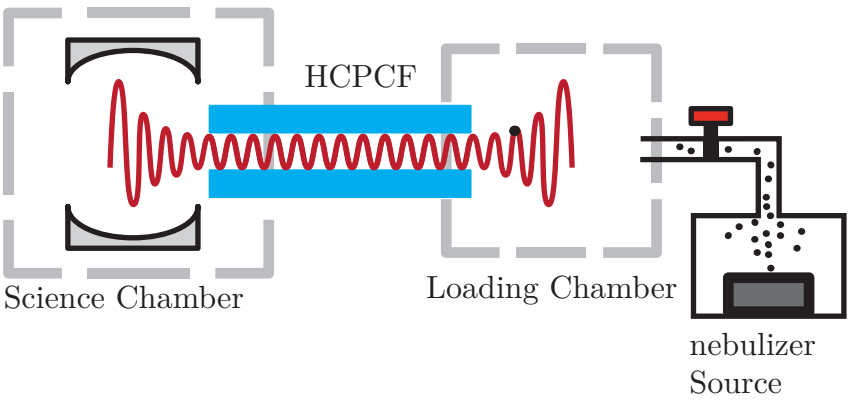

Figure 3: Novel loading mechanism for nanoparticles

Figure 3 shows the setup for a novel particle source. It combines the advantages of nebulizer sources with optical tweezers and hollow core photonic crystal fibers (HCPCF).

A HCPCF is a fiber which supports Gauss like light propagating in an hollow core filled with air. The size of the air core can be tens of micrometers and is therefore large enough to allow transport of nanoparticles. One end of the HCPCF is placed in a science chamber with an UHV environment. The second end is placed in a loading chamber connected with an nebulizer particle source. Light is coupled into the fiber from both sides with equal polarisations building a standing wave through the entire HCPCF and in front of the fiber ends. Particle-solvent fog from the evaporative source is sucked via a tube into the loading chamber and eventually a particle will be trapped in front of the HCPCF. Moving the whole standing wave with the trapped particle through the HCPCF into the science chamber allows a transport of a single particle from the loading chamber into the science chamber at a desired place, where the fiber ends.

Compared to piezoelectric sources and only nebulizer sources this method provides several advantages. It supports all particle sizes which can be nebulized and which can be held in the optical trap. Secondly it is a particle source which allows control over the amount of particles transported into the science chamber and it can deliver particles at a well defined position. This is a huge advantage compared to the randomness of particle number and position of other sources. It is also a UHV compatible source as it does not contaminate the science chamber. All evaporative processes are done in the loading chamber.

1.3. Throughput of a hollow core photonic crystal fiber

To use this novel source in a UHV experiment one has to assure that the hollow core fiber connecting the loading chamber with the science chamber allows sufficiently high pressure difference. The flow of air through the core has to be small enough to keep a good vacuum in the science chamber. In general, the flow through tubes, or a hollow core fiber in this particular case, is classified in three different regimes: molecular flow, Knudsen flow and continuous flow. Molecular flow describes a regime where the mean free path length of the gas molecules is large compared to the geometry of the system, namely the tube radius. The motion of molecules is dominated by their inertia and scattering with walls. The continuous regime is dominated by collisions of molecules with each other where the mean free path length is much smaller than the dimensions of the system. Knudsen flow describes the intermediate regime. The Knudsen number $\mathrm{Kn} = \frac{l}{2R}$ with R the tube radius, $l = \frac{k_B T}{\pi\sqrt{2}\sigma_g p}$ the mean free path length, k_B the Boltzmann constant, T the temperature of the gas, σ_g the cross section of a gas molecule and p the gas pressure classifies the different regimes. A Knudsen number $\mathrm{Kn} > 0.5$ describes molecular flow, $0.5 > \mathrm{Kn} > 0.01$ Knudsen flow and $0.01 > \mathrm{Kn}$ laminar flow. The Knudsen number for a tube with $R = 5 \times 10^{-6}$m, the core radius of the HCPCF used in this experiment, and air at room temperature is plotted against the pressure in figure 4. Assuming the loading chamber at room pressure (1000mbar) and the science chamber at $p = 10^{-4}$mbar one sees that the flow undergoes already all three regimes as the Knudsen number varies from $10^{-4} < \mathrm{Kn} < 100$. Standard vacuum technology calculations, see [23] for example, offer estimations for a system undergoing all three regimes. It can be described by two parallel tubes in which one only laminar flow takes place and in the

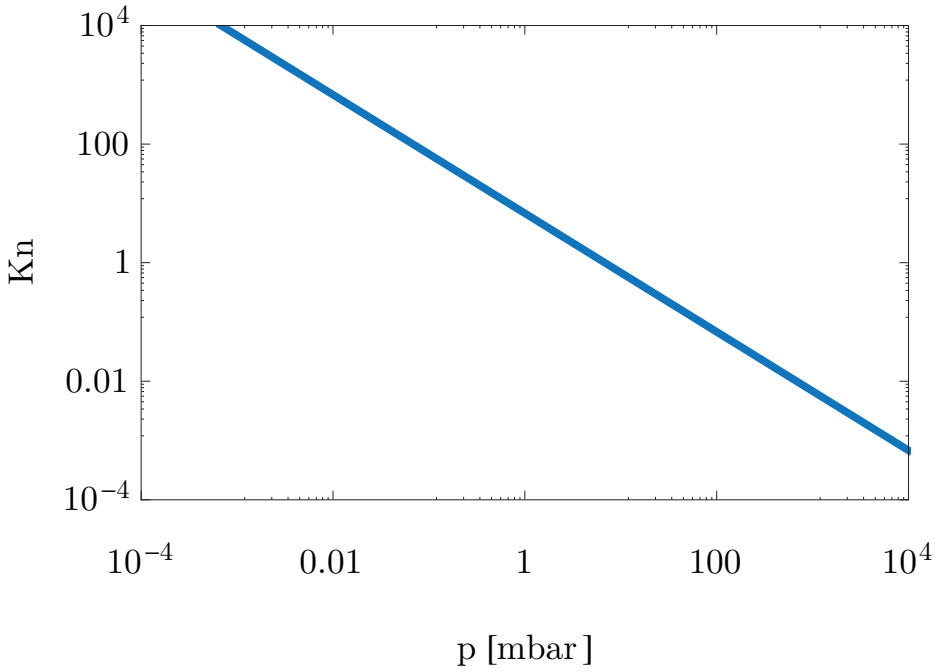

Figure 4: Knudsen number Kn for a tube with 10μm diameter depending on the pressure p

other tube just molecular flow. The overall flow adds up. Therefore, the flow of gas from a high pressure region (loading chamber) through a hollow core fiber into a low pressure region (science chamber) connected with a pumping system can be estimated. The final pressure in the science chamber is given by an equilibrium of the flow into the chamber via the hollow core fiber and the outflow by the vacuum pump.

Vacuum pumps have a constant, device specific, volume flow rate $S = \frac{dV}{dt}$. The throughput of a pump is $Q_{\text{Pump}} = Sp$ with p the pressure at which the pump is operating. It describes the outflow of gas by the pump. The throughput in the continuous (molecular) regime through a tube of length l and radius R is given by [23]

$$Q_{\text{lam}} = \frac{\pi(2R)^4}{256\eta l}(p_L^2 - p_S^2)$$
$$Q_{\text{mol}} = \frac{(2R)^3}{l} c_T(p_L - p_S)$$

with c_T the mean thermal velocity of the gas, η the viscosity of the gas, p_S and p_L the pressure in the science and loading chamber. Figure 4 shows a plot of the throughput for a HCPCF (blue curve) and a vacuum pump (red curve) depending on pressure. The loading chamber was assumed to operate at room pressure, a fiber length of $l = 10$cm and a vacuum pump with a volume flow rate $S = 0.05\frac{\text{m}^3}{s}$. The throughput of the HCPCF is almost constant as the difference between room pressure and a small pressure

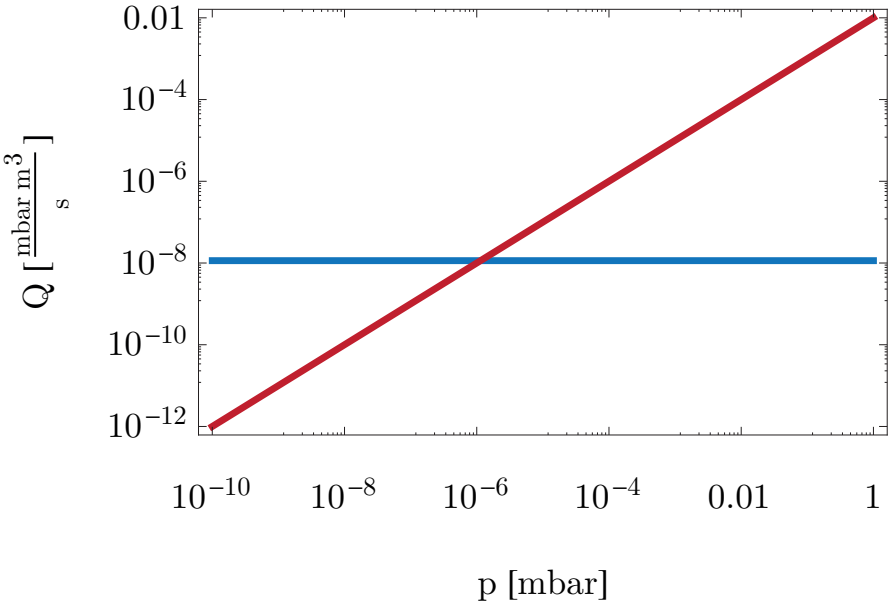

Figure 5: Throughput Q of a HCPCF (blue curve) with one end free space (room pressure), the second end at pressure p and throughput Q of vacuum pump (red curve) operating at pressure p

is negligible. The intersection of both curves gives the equilibrium pressure, the lowest pressure achievable in the science chamber for this configuration. The throughput of the vacuum pump is just sufficient to compensate the throughput into the chamber via the HCPCF. In this case a pressure difference from room pressure to $p \approx 10^{-6}$mBar, nine orders of magnitude, is achievable.

There are two possibilities to increase the pressure difference even further. One can prolong the length of the HCPCF as the throughput decreases inverse proportional in fiber length. Note that the same can be done with a better vacuum pump. An increase by at least a factor 40 in volume flow rate[2] is current state of the art vacuum technology.

A second way to decrease the pressure in the science chamber can be done with a third, intermediate vacuum chamber between loading and science chamber connected via a HCPCF. The two HCPCF endings in the intermediate chamber can be butt coupled[3], acting as floodgate. A pressure difference of nine orders of magnitude from loading chamber to intermediate chamber, as described before, provides a pre-vacuum. It can, in principle, be increased by the same order of magnitude with a HCPCF from the intermediate to the science chamber.

This estimation for maximum achievable pressure difference is questionable as gas flow

[2]compared to $S = 0.05\frac{\text{m}^3}{s}$

[3]Butt coupling means bringing two fiber ends so close to each other that no additional optics are required to couple light from one fiber into the other. A particle can then be transported from one fiber into the other

in micrometer sized tubes seems to behave differently as in macroscopic vacuum tubes. According to [24] for low pressures and therefore few gas molecules, the continuum based Navier-Stokes equations reach their limits. That is why a small experiment with a 10cm piece HCPCF and a vacuum pump with a volume flow rate $S = 0.05\frac{\mathrm{m}^3}{s}$ was done to verify the estimations shown in figure 5. The fiber was glued with epoxy in a vacuum flange and connected with a pressure sensor and the vacuum pump. The other end of the fiber was at room pressure. Pumping down the system for one day lead to a final pressure of $p = 4.7 \times 10^{-6}$mbar. This was the limit of the vacuum system used. In order to find the real cutoff pressure, a better vacuum system would have been required, which was not available at that point. The intersection point predicted by the two curves in figure 5 at $p = 1 \times 10^{-6}$mbar has however almost been reached demonstrating the possibility to bridge nine orders of magnitude in pressure.

Loading nanoparticles with a nebulizer source at 1mbar has been demonstrated, see [11], so the throughput of the HCPCF is not to be expected to be the limiting factor in achieving the required 10^{-7}mbar for groundstate cooling.

2. Optical Trapping

Light can be used to control the motion of small dielectric particles. The first experiments were done by Ashkin [14, 25, 15, 26] in the early seventies. Since this pioneering works optical trapping has been used for many different applications in different fields of research. With this techniques trapping of atoms with light was realized or Biologists, to give another example, use optical trapping to investigate biomolecules, DNA, proteins etc. The review [27] and the book [26] summarizes applications of optical trapping for further reading.

This chapter introduces the basics for optical trapping of small dielectric particles in a Gaussian light field which can describe the optical trap for nanoparticles built with a HCPCF.

2.1. Gaussian Beam

The electrical field amplitude of a Gaussian TEM00 mode propagating along the z-axis is described by

$$\begin{aligned}\vec{E}(\vec{r},t) &= E_0 \frac{\omega_0}{\omega(z)} e^{-i(kz+2\pi\nu t)} e^{-\frac{x^2+y^2}{\omega^2(z)}} e^{-ik\frac{x^2+y^2}{2R(z)}} e^{i\zeta(z)} \cdot \vec{p}\, e^{-i2\pi\nu t} \\ &= E(r,z) \cdot \vec{p}\, e^{-i2\pi\nu t}\end{aligned} \tag{2}$$

with $\omega(z) = \omega_0\sqrt{1+\left(\frac{z}{z_R}\right)^2}$ the waist, ω_0 the minimal waist, $z_R = \frac{\pi\omega^2}{\lambda}$ the Rayleigh length, λ, ν the wavelength and the frequency of light, $k = \frac{2\pi}{\lambda}$ the wave number, $R(z) = z\left[1+\left(\frac{z_R}{z}\right)^2\right]$ the radius of curvature of wave fronts, $\zeta(z) = \arctan(\frac{z}{z_R})$ the Gouy phase, $r = \sqrt{x^2+y^2}$ the radius in polar coordinates and $\vec{p}$ the polarisation vector.

For non-conducting and non-magnetic materials, especially air and silica, the refractive index can be written as $n^2 \approx \varepsilon/\varepsilon_0$ with ε the dielectric constant of the material and $\varepsilon_0 = 8.8510^{-12}\frac{\mathrm{F}}{\mathrm{m}}$ the vacuum permittivity. The magnetic permeability can be assumed as $\mu = \mu_0$ with the magnetic permeability of vacuum.

The magnetic field is $\vec{H}(\vec{r},t) = n_2\varepsilon_0 c\, \vec{e}_z \times \vec{E}(\vec{r},t)$ with n_2 the refractive index of the medium in which the wave propagates and c the speed of light. The Intensity is the time average of the pointing vector

$$\begin{aligned}\vec{I}(r,z) &= \left\langle \vec{S} \right\rangle_T \\ &= \left\langle \vec{E} \times \vec{H} \right\rangle_T \\ &= n_2\varepsilon_0 c |\vec{E}(r,z)|^2 \cdot \vec{e}_z \, \frac{1}{T}\int_0^T dt e^{-4\pi\nu t} \\ &= \frac{n_2\varepsilon_0 c}{2} |\vec{E}(r,z)|^2 \cdot \vec{e}_z \\ &= \frac{2P}{\pi\omega(z)^2}\, e^{-2\frac{r^2}{w(z)^2}} \cdot \vec{e}_z\end{aligned}$$

with $P = \frac{1}{4}\pi\omega_0^2 n_2 \varepsilon_0 c E_0^2$ the power as defined in [28].

2.2. Standing Wave

Superimposing two counter propagating electrical fields with the same polarisation vectors $\vec{p_1} = \vec{p_2}$ leads to a standing wave. Both light beams are assumed to have the same waist ω_0, same electric field amplitude $E_1 = E_2 = E$ and the same frequency ν. The intensity is proportional to the superposition of the electric fields $\vec{E}_1$ and $\vec{E}_2$ square

$$\begin{aligned} I(r,z) &\propto |\vec{E}_1^2(\vec{r},t) + \vec{E}_2^2(\vec{r},t)|^2 \\ &= |E_1^2(r,z) + E_2^2(r,z)|^2 \\ &= E^2 \frac{\omega_0^2}{\omega^2(z)}\ e^{-\frac{r^2}{\omega^2(z)}} \Big|\ e^{-ikz} e^{-ik\frac{r^2}{2R(z)}} + e^{ikz} e^{ik\frac{r^2}{2R(z)}} \Big|^2 \\ &= E^2 \frac{\omega_0^2}{\omega^2(z)}\ e^{-\frac{r^2}{\omega^2(z)}}\ 4\cos^2\left[k\Big(z + \frac{r^2}{2R(z)}\Big)\right]. \end{aligned}$$

The intensity of the standing wave is given by

$$\begin{aligned} I(r,z) &= \frac{n_2 \varepsilon_0 c}{2}\ E^2 \frac{\omega_0^2}{\omega^2(z)}\ e^{-\frac{r^2}{\omega^2(z)}}\ 4\cos^2\left[k\Big(z + \frac{r^2}{2R(z)}\Big)\right] \\ &= \frac{8P}{\pi\omega^2(z)}\ e^{-\frac{r^2}{\omega^2(z)}}\ \cos^2\left[k\Big(z + \frac{r^2}{2R(z)}\Big)\right]. \end{aligned} \tag{3}$$

The waist ω_0 is small compared to the radius of curvature $R(z)$. Thus we can neglect the second argument of the cosine function in equation 3 and write the intensity of a standing wave

$$I(r,z) = \frac{8P}{\pi\omega^2(z)}\ e^{-\frac{r^2}{\omega^2(z)}}\ \cos^2(kz). \tag{4}$$

The intensity is strongest along the z-axis and has a maximum at $z = 0$ where the waist is smallest. It is periodic along z-direction with half the wavelength of the light.

2.3. Radiation Forces and Harmonic Potential

The interaction between a small dielectric particle and light can be described with Rayleigh theory if the particle radius a is smaller than the wavelength $a \ll \lambda$. In this regime one can separate the radiation force in two components, scattering force and gradient force.

As the particle is smaller than the wavelength it can be treated as a point dipole. The electromagnetic field polarizes the dielectric particle and drives it with the frequency ν. The induced dipole therefore starts radiating, or scattering. Every photon from the incident light impinging the sphere is either absorbed or scattered and therefore

transferring momentum from the light to the particle. The overall change of momentum leads to a force on the particle in direction of the light propagation, the scattering force

$$\vec{F}_{scatt}(r,z) = \frac{n_2}{c}\sigma_{scatt} I(r,z) \cdot \vec{e}_z \tag{5}$$

with $\sigma_{\text{scatt}} = \frac{8}{3}\pi k^4 a^6 \left(\frac{u^2-1}{u^2+2}\right)^2$ the scattering cross section of a dielectric particle in the Rayleigh regime [28] and $u = n_a/n_2$ with n_a the refractive index of the particle.

On the other hand, a Lorentz force acts on a dipole in an electromagnetic field. It pushes the particle along the field gradient towards a field extrema and is given by [28]

$$\vec{F}_{grad}(r,z) = \frac{2\pi n_2 a^3}{c}\frac{u^2-1}{u^2+2}\nabla I(r,z). \tag{6}$$

The gradient force is proportional to the volume of the particle, independent of the wavelength and points always in direction of the strongest field gradient. The gradient force is conservative with the potential

$$U(r,z) = -\frac{2\pi n_2 a^3}{c}\frac{u^2-1}{u^2+2}\, I(r,z) \tag{7}$$

as the force of any conservative potential can be written as the negative gradient of a scalar function. Two counter propagating beams have the same intensity if we choose them to have equal power, waist and frequency. Therefore the scattering force from the left and the right beam cancel. The remaining gradient force can then be calculated from the intensity of the superimposed electrical fields given by equation 4. Figure 6

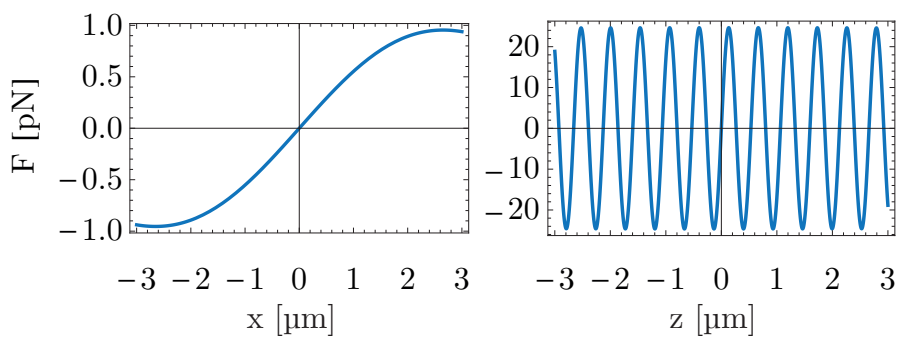

Figure 6: Gradient force of a standing wave trap ($P = 2$W, $\omega_0 = 3.75\mu$m) on a silica sphere depending on the radial x-position (left) and the axial z-position (right)

shows the forces on a Rayleigh particle in a standing wave. It is instructive to point out that a force of 1pN on a 127nm silica sphere corresponds to an acceleration of $44000\frac{\text{m}}{\text{s}^2}$.

The left part shows the force along x-direction at z=0. A particle close to the origin will always be attracted towards the beam centre, the equilibrium position where $F = 0$. If perturbations from the equilibrium position are small enough the particle returns as the force points in the opposite direction as the displacement. The same argument holds for the equivalent y-direction. In this context we have a "stable trap" in x- and y-direction.

The right part in figure 6 shows the force of a standing wave acting on a small particle along the z-axis. The main difference compared to forces along x,y-directions is its periodicity, there are more than just one trap position. If a particle is trapped at one particular equilibrium position ($F_{\mathrm{grad,z}} = 0$) the behaviour for perturbations from the equilibrium position is the same as for the other directions.

The gradient force along z-direction is strongest as the field gradient in z-direction is higher than in x,y direction.

For a particle is trapped in a standing wave the potential can be approximated with a Taylor expansion for small displacements

$$U(x,y,z) \approx U(0) + \sum_i \left.\frac{\partial U(x,y,z)}{\partial x_i}\right|_{x,y,z=0} x_i + \sum_i \left.\frac{\partial^2 U(x,y,z)}{\partial x_i^2}\right|_{x,y,z=0} x_i^2. \tag{8}$$

The second term in equation 8 is zero and we neglect terms of order $O(x_i^3)$. The resulting potential describes a three dimensional harmonic oscillator. Properties of the trap can now be related to properties of a harmonic oscillator. The coefficients in the quadratic term $\kappa_i := \frac{\partial^2 U(x,y,z)}{\partial x_i^2}$ are the spring constants for each direction. The trap frequencies Ω_i with $i = x, y, z$ are $\Omega_i = \sqrt{\frac{\kappa_i}{m}}$ with m the mass of the trapped particle. The constant $U(0)$ is the trap depth and tells how much kinetic energy a particle needs to escape the trap.

The radial frequencies are given by

$$\Omega_{x,y} = \sqrt{\frac{24 P n_2}{\pi w_0^4 c \rho}\left(\frac{u^2-1}{u^2+2}\right)}$$

and the axial frequency is

$$\Omega_z = \sqrt{\frac{P n_2}{\pi c \rho}\left(\frac{u^2-1}{u^2+2}\right)\left(\frac{12\lambda^2}{\pi^3 \omega_0^6} + \frac{96\pi}{\lambda^2 \omega_0^2}\right)}. \tag{9}$$

The frequencies for a Rayleigh particle are independent of mass or size and just depend on the density ρ of the particle and the ratio of refractive index of particle and surrounding medium u.

2.4. Damping

The gradient force, as described in chapter 2.3 is conservative and therefore not capable of capturing a particle. Any particle entering the trap gains the kinetic energy U_0 and this is, by definition, sufficient to leave the trap again. The surrounding air provides at

reasonable pressure sufficient damping to trap particles in a conservative potential. The damping rate for a rarefied gas and a spherical particle is given by [29, 30, 31]

$$\gamma = \frac{6\pi\eta a}{m}\frac{0.619}{0.619 + \mathrm{Kn}}(1 + c_{\mathrm{K}}) \tag{10}$$

with η the viscosity of the surrounding medium, $c_{\mathrm{K}} = \frac{0.31\mathrm{Kn}}{0.785+1.152\mathrm{Kn}+\mathrm{Kn}^2}$ a correction factor for higher pressures, l the mean free path of the gas molecules and $\mathrm{Kn} = \frac{l}{a}$ the Knudsen number[4]. The mean free path is $l = \frac{k_{\mathrm{B}}T}{\pi\sqrt{2}\sigma_g p}$ with σ_g the molecule cross section and p the pressure of the gas. Figure 7 shows the damping rate for a silica nanosphere with a

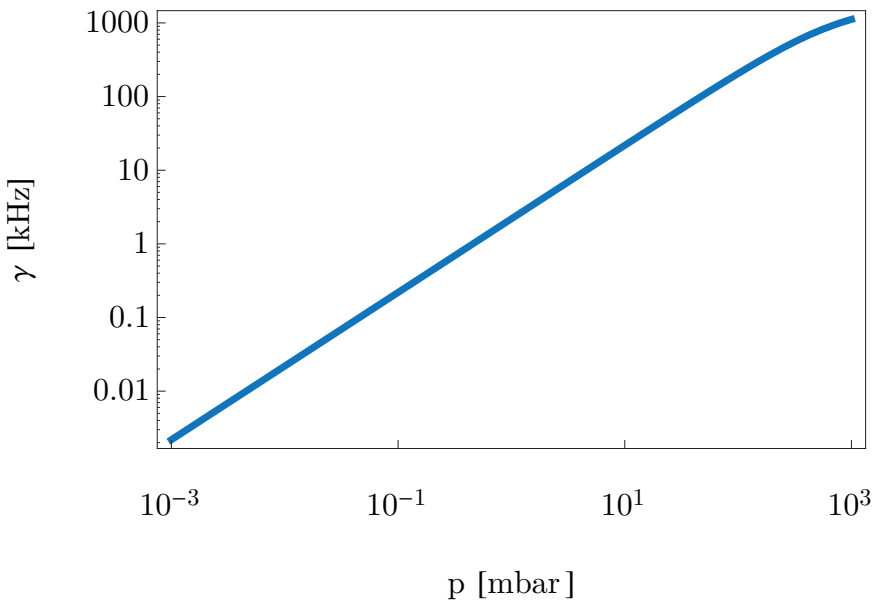

Figure 7: Damping rate γ for a 127nm silica sphere in air depending on pressure

radius $a = 127$nm in air. For low pressures the damping is proportional to the pressure of the surrounding gas.

The equation of motion for a free, damped harmonic oscillator is $\ddot{x} + \gamma\dot{x} + \Omega^2 x = 0$. There exist three qualitative different solutions. The first solution is the underdamped case where the damping $\gamma < 2\Omega$ is smaller as double the mechanical frequency. The system oscillates with an exponential decaying envelope. Secondly, there is the overdamped case $\gamma > 2\Omega$ where the system does not oscillate at all. If excited it decays without oscillation into the groundstate. And the third case where $\gamma = 2\Omega$, the critical damped case, the system can oscillate once and then go back into the ground state, but faster as the overdamped system would.

A quantity commonly used to characterize a harmonic oscillator is the Q factor. It is defined as $\mathrm{Q} := \frac{\Omega}{\gamma}$ the ratio of mechanical frequency and damping rate. According

[4]Knudsen number describing a sphere in air

to the under-, over- and critical damped system the Q factor is bigger, smaller or equal to $\frac{1}{2}$. For an underdamped oscillator Q is the number of oscillations till the system lost half of its energy by the damping process.

2.5. Noise Power Spectrum of a Harmonic Oscillator

The whole system consisting of the harmonic potential introduced by the electromagnetic field, a trapped nanoparticle and the surrounding gas can be described with Langevin equations as in [32, 33, 21, 34]. Harmonic potential and damping were introduced in the former chapters but the interaction of the sphere with the environment is still incomplete. The surrounding air with a finite temperature T is responsible for a random force noise $F_t = \sqrt{2k_\mathrm{B}T\gamma m}\,\zeta(t)$ describing the coupling to the thermal environment. $\zeta(t)$ is a white noise process vanishing for time averaging $\langle\zeta(t)\rangle = 0$ and is uncorrelated $\langle\zeta(t)\zeta(s)\rangle = \delta(t-s)$. It is the origin of a random motion of the particle caused by scattering with surrounding fast moving molecules or atoms. It is linked to the temperature and the damping of the surrounding medium as it contains their dynamic properties. All three spatial directions are uncoupled so the problem is only treated in one dimension

$$\ddot{x} + \gamma\dot{x} + \Omega^2 x = \frac{F_t}{m} \tag{11}$$

with γ the damping rate and Ω the mechanical frequency of the particle.

Equation 11 can be solved by applying a Fourier transformation. The time derivative transforms to a multiplication with $i\omega$ in Fourier space and the Fourier transform of the displacement is $\tilde{x}(\omega) = \int dt\; e^{-i\omega t}x(t)$

$$-\omega^2\tilde{x}(\omega) + i\omega\gamma\tilde{x}(\omega) + \Omega^2\tilde{x}(\omega) = \frac{\tilde{F}_t}{m}. \tag{12}$$

The displacement in Fourier space is then

$$\tilde{x}(\omega) = \frac{\tilde{F}_t}{m}\frac{1}{\Omega^2 - \omega^2 + i\omega\gamma}$$

and the spectrum of a harmonic oscillator is defined as

$$\begin{aligned} S_{xx}(\omega) &= \langle|\tilde{x}(\omega)|^2\rangle \\ &= \frac{2k_\mathrm{B}T\gamma}{m}\frac{1}{(\Omega^2-\omega^2)^2+\omega^2\gamma^2}. \end{aligned} \tag{13}$$

Any experimentally measured spectrum has a finite bandwith, thus the Fourier transformation applied in equation 12 is in fact a Fourier series and the measured spectrum always contains noise of the Brownian stochastic force. Integrating the spectrum over all frequencies

$$\begin{aligned} \int_0^\infty d\omega\; S_{xx}(\omega) &= \frac{2k_\mathrm{B}T\gamma}{m}\int_0^\infty d\omega\; \frac{1}{(\Omega^2-\omega^2)^2+\omega^2\gamma^2} \\ &= \pi\frac{k_\mathrm{B}T}{m\Omega^2} \end{aligned} \tag{14}$$

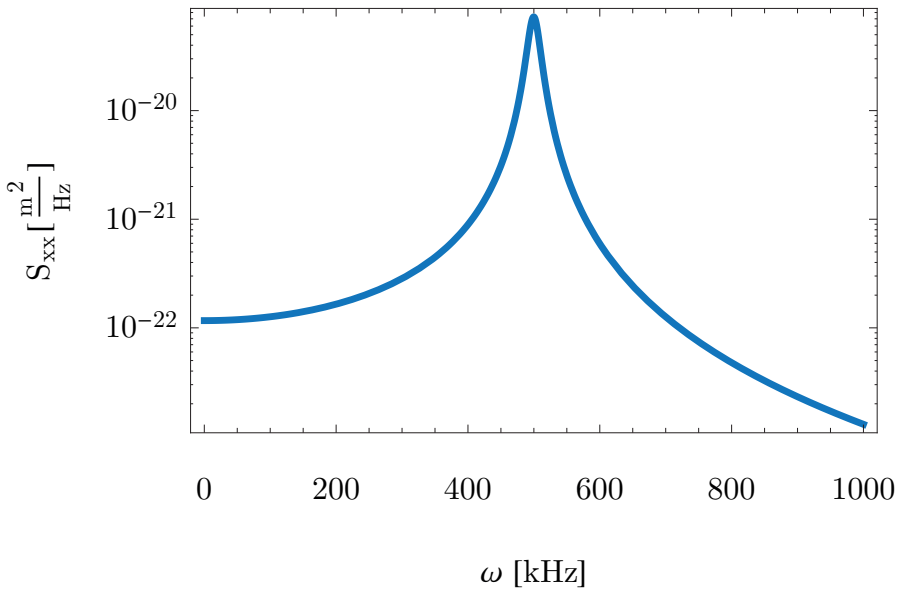

Figure 8: Spectrum S_{xx} of a harmonic oscillator with a mechanical frequency $\Omega = 500$ kHz and a dampingrate $\gamma = 20$ kHz which corresponds to $Q = 25$

leads to the temperature of a harmonic oscillator. Figure 8 exemplary shows the spectrum of a harmonic oscillator[5].

Once one has access to the spectrum of an oscillator, fitting equation 13 gives the mechanical frequency, the damping and the temperature of the system.

2.6. Position Detection

To measure the spectrum of an optically trapped particle a position read out is necessary.

One method is based on interference of light from the trap, which provides a phase reference, with scattered light from the trapped particle which contains an additional phase due to its motion. Figure 9 shows a sketch for a interference based readout of the particle motion. The particle moves in the trap and is at a certain time displaced by $\Delta\vec{r}$ from the potential maximum (equilibrium position). A detector (screen) far away from the trapped particle measures the power of the incoming light. If we approximate the dipole radiation with a spherical wave and the TEM00 mode with plane waves the interference signal is proportional to

$$I(\vec{r}) \sim |E_0 e^{i(k_z z - \frac{\pi}{2})} + E_D e^{i\vec{k}(\vec{r}-\Delta\vec{r})}|^2$$

with E_0 the amplitude of the incident electric field, E_D the amplitude of the scattered field by the sphere and $\Delta\vec{r}$ the displacement of the particle. The electric field providing

[5] with a mechanical frequency of $\Omega = 500$ kHz and a damping $\gamma = 20$ kHz

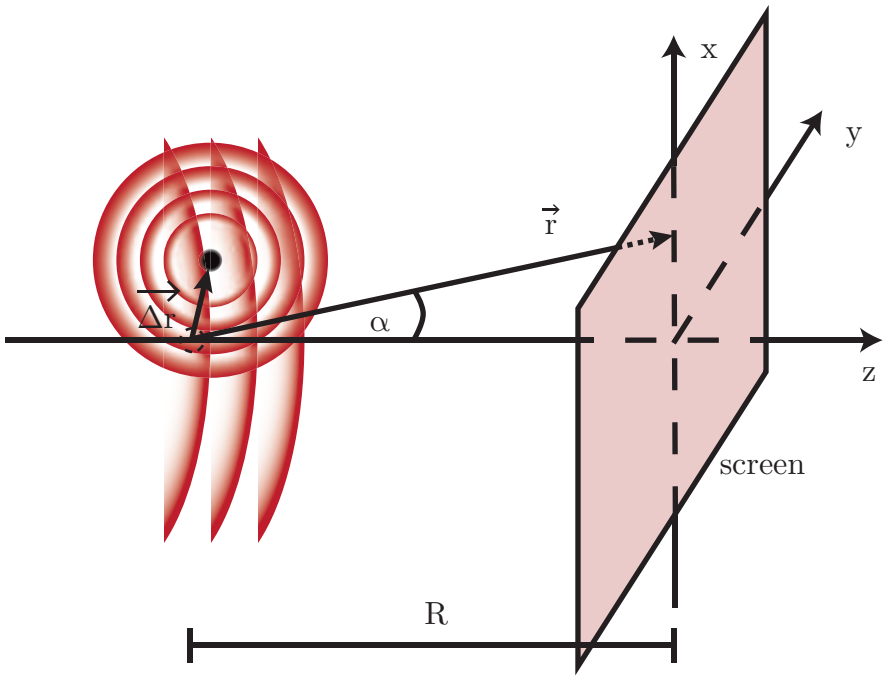

Figure 9: Position detection based on interference of trapping light with scattered light of a nanosphere

the phase reference gathers an additional phase, the Gouy phase $\zeta = -i\frac{\pi}{2}$ far away from the origin $R \gg z$ whereas the dipole radiation does not. The intensity can be measured with a detector positioned like the screen in figure 9. Let's assume the detector to be on axis at $z = R$ and the size of the active area of the detector $x_0, y_0 \ll R$ smaller than the distance between detector and particle. From geometrical considerations one gets $\frac{x_i}{z} = \frac{k_{x_i}}{k_z}$ for $i = x, y$ and then the intensity is proportional to

$$\begin{aligned} I(x, y, z = R) &\sim |E_0 e^{i(k_z z - \frac{\pi}{2})} + E_D e^{i\vec{k}(x\cdot\vec{e}_x + y\cdot\vec{e}_y + R\cdot\vec{e}_z - \vec{\Delta r})}|^2 \\ &= |E_0 e^{i(k_z z - \frac{\pi}{2})} + E_D e^{i\left[k_z R(\frac{x^2}{R^2} + \frac{y^2}{R^2} + 1) - \frac{k_z}{R}(x\Delta x + y\Delta y + R\Delta z)\right]}|^2 \\ &\approx |E_0 e^{i(k_z z - \frac{\pi}{2})} + E_D e^{i\left[k_z R - \frac{k_z}{R}(x\Delta x + y\Delta y + R\Delta z)\right]}|^2 \\ &= E_0^2 + E_D^2 + 2E_0 E_D \sin\left[\frac{k_z}{2R}(x\Delta x + y\Delta y + R\Delta z)\right]. \end{aligned} \tag{15}$$

The approximation in the third line of equation 15 is valid as we are just interested in intensities on the detector area $x \leq x_0$, $y \leq y_0$.

The position in the z-direction can be determined from the on-axis intensity at the detector. Figure 10 shows a schematic of an axial position detection. Let's assume the sphere is displaced by the distance Δz from an intensity maxima and calculate power P

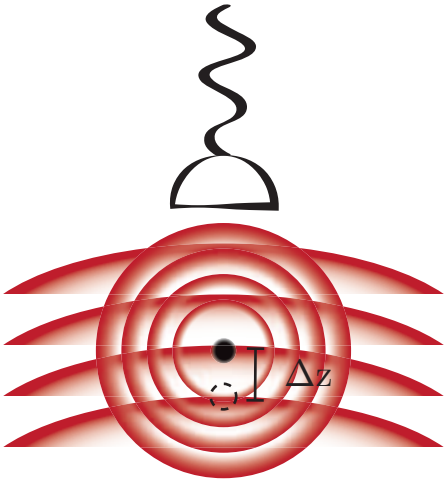

Figure 10: Position readout along z-direction of a trapped nanoparticle displaced by Δz

on the detector.

$$
\begin{aligned}
P &= \int_{-y_0}^{y_0} dy \int_{-x_0}^{x_0} dx \; I(x, y, z = R) \\
&\propto 4 \frac{R^2}{k_z^2 \Delta x \Delta y} \sin\left(\frac{k_z x_0 \Delta x}{2R}\right) \sin\left(\frac{k_z y_0 \Delta y}{2R}\right) \sin\left(\frac{k_z \Delta z}{2}\right) \\
&\approx \frac{x_0 y_0 k_z}{2} \; \Delta z.
\end{aligned}
\tag{16}
$$

The detected signal is proportional to the displacement along the z direction $P \propto \Delta z$.

With this method an axial position readout of a particle motion is possible. Experimental implementation of this detection method has been for example realized in [31],[30].

3. Hollow Core Photonic Crystal Fibers

In this chapter hollow core photonic crystal fibers (HCPCF) will be introduced, which are a progression of standard single mode fibers (SMF). They guide a light mode inside the hollow core which allows trapping and guidance of nanoparticles from a loading chamber into a science chamber.

Figure 11 shows an example of a HCPCF surface. The inner air core is surrounded by a periodic arrangement of air holes, the photonic crystal cladding, which is again surrounded by a silica cladding. In contrast to SMF fibers which consists just of two materials, a core and a surrounding cladding with refractive indices n_{co} and n_{cl}. Light facing a change of refractive index, for example light in a SMF impinging from the core to the cladding, is described by Snell's law $\sin\theta_{\mathrm{co}} n_{\mathrm{co}} = \sin\theta_{\mathrm{cl}} n_{\mathrm{cl}}$. For $n_{\mathrm{co}} < n_{\mathrm{cl}}$ it follows that $\sin\theta_{\mathrm{co}} < n_{\mathrm{cl}}/n_{\mathrm{co}} < 1$ and therefore $\theta_{\mathrm{co}} < \arcsin n_{\mathrm{cl}}/n_{\mathrm{co}}$. If $\sin\theta_{\mathrm{co}}$ overcomes this angle there will be no light refracted and all the light must be reflected (total internal reflection, TIR). Based on TIR it is impossible to have a SMF with an air core as there is no material with a lower refractive index than air for optical frequencies. Instead one replaces the cladding with a photonic crystal which traps light in the core such that no TIR guiding mechanism is needed any more. HCPCF are a particular species of

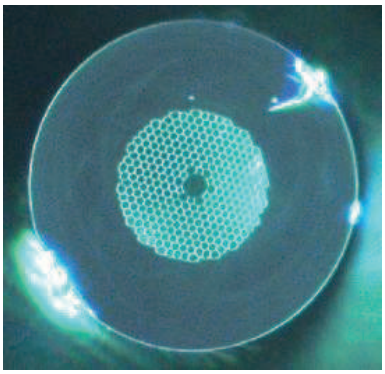

Figure 11: Dark field image of a HC1060 HCPCF from NKT Photonics

photonic crystal fibers (PCF). PCF mainly consist of a photonic crystal in the centre and a silica cladding. The structure of the photonic crystal differs depending on their purpose, in the simplest form it is just an array of small holes. In this sense a HCPCF is a PCF with an defect in the centre, the air core.

3.1. Photonic Crystals

In general photonic crystals are periodic dielectric structures of the order of the length-scale of the wavelength they are designed for. Photonic crystal produce photonic band gaps which forbid certain frequencies to propagate and allow others to do so. A good introduction to photonic crystals can be found in [35] which is also the basis for this brief

introduction. The macroscopic Maxwell equations without free charges and currents are

$$\nabla \cdot \vec{B} = 0 \qquad \nabla \times \vec{E} + \partial_t \vec{B} = 0$$
$$\nabla \cdot \vec{D} = 0 \qquad \nabla \times \vec{H} - \partial_t \vec{D} = 0$$

with $\vec{E}$ and $\vec{H}$ the macroscopic electric and magnetic fields, $\vec{D}$ and $\vec{B}$ the displacement and the magnetic induction fields. The displacement field $\vec{D}$ and the electric field are related via

$$\frac{D_i}{\varepsilon_0} = \sum_i \varepsilon_{ij} E_j + \sum_{j,k} \chi_{ijk} E_j E_k + O(E^3)$$

with $\varepsilon_0 = 8.8510^{-12}$ Farad/m the vacuum permittivity. We neglect nonlinear terms and consider just macroscopic, isotropic, transparent materials. That means that $\vec{D}(\vec{r}) = \varepsilon_0 \varepsilon(\vec{r}) \vec{E}(\vec{r})$ with $\varepsilon(\vec{r})$ a scalar, real and positive relative permittivity. We also assume dispersion free materials $\varepsilon(\vec{r}, \omega) = \varepsilon(\vec{r})$ as we are just interested in small frequency ranges. Similar approximations are made for the magnetic field. As most relative magnetic permeabilities $\mu(\vec{r})$ are close to 1 one may write $\vec{B} = \mu_0 \vec{H}$. With this approximations one can relate the refractive index with the relative permittivity via $n^2 = \varepsilon/\varepsilon_0$. This simplifies Maxwell equations to

$$\nabla \cdot \vec{H} = 0 \tag{17}$$
$$\nabla \times \vec{E} + \mu_0 \, \partial_t \vec{H} = 0 \tag{18}$$
$$\nabla \cdot \vec{E} = 0 \tag{19}$$
$$\nabla \times \vec{H} - \varepsilon_0 \varepsilon(\vec{r}) \, \partial_t \vec{E} = 0. \tag{20}$$

The Maxwell equations are linear differential equations and fulfil the superposition principle. It allows an Ansatz in Fourier modes and decouples spatial from time derivatives

$$\begin{aligned} \vec{H}(\vec{r}, \omega) &= \vec{H}(\vec{r}) e^{-i\omega t} \\ \vec{E}(\vec{r}, \omega) &= \vec{E}(\vec{r}) e^{-i\omega t}. \end{aligned} \tag{21}$$

Inserting this Ansatz in equation 20 and equation 19, and combining those results gives the Master equation

$$\nabla \times \left[\frac{1}{\varepsilon(\vec{r})} \nabla \times \vec{H}(\vec{r}) \right] = \Theta \vec{H}(\vec{r}) = \left(\frac{\omega}{c} \right)^2 \vec{H}(\vec{r}) \tag{22}$$

The operator Θ (Master Operator) on the left side of equation 22 is Hermitian[6]. Therefore all well known mathematical tools for solving hermitian Eigenvalue equations can be used. To give on example as in quantum mechanics there exist a variational theorem to determine to lowest frequency (or energy) eigenmode, the Rayleigh quotient

$$U_f(\vec{H}) = \frac{\langle \vec{H}, \Theta \vec{H} \rangle}{\langle \vec{H}, \vec{H} \rangle}.$$

[6]that is the main reason why we are using the H field instead of the E field

It is minimal for the lowest frequency eigenmode $\vec{H}_0$. Inserting the Ansatz from equation 21 into Maxwell equation 19 replaces the $\vec{H}$ field with the $\vec{E}$ field. Thus the Rayleigh quotient changes to

$$\begin{aligned} U_f(\vec{E}) &= \frac{\langle \nabla \times \vec{E}, \vec{E} \nabla \times \vec{E} \rangle}{\langle \vec{E}, \varepsilon(\vec{r}) \vec{E} \rangle} \\ &= \frac{\int d\vec{r}\, |\nabla \times \vec{E}(\vec{r})|^2}{\int d\vec{r}\, \varepsilon(\vec{r}) |\vec{E}(\vec{r})|^2} \end{aligned} \tag{23}$$

To minimise this functional one has to find modes which have high field amplitudes in the high $\varepsilon(\vec{r})$ regions to maximise the denominator and modes with few spatial oscillations to minimise the numerator. As we are looking at a Hermitian operator we know that different eigenmodes are orthogonal to each other. If one finds the lowest frequency eigenmode $\vec{H}_0$ the next higher mode minimises the Rayleigh quotient in an orthogonal subspace to $\vec{H}_0$.

3.2. Symmetries

A useful tool to characterize the modes of photonic crystals are symmetries. In case of photonic crystal fibers there is a continuous translation symmetry along the fiber axis and discrete translation symmetries in transversal direction provided by the photonic crystal cladding [7]. A continuous translation symmetry means that a system shifted about any

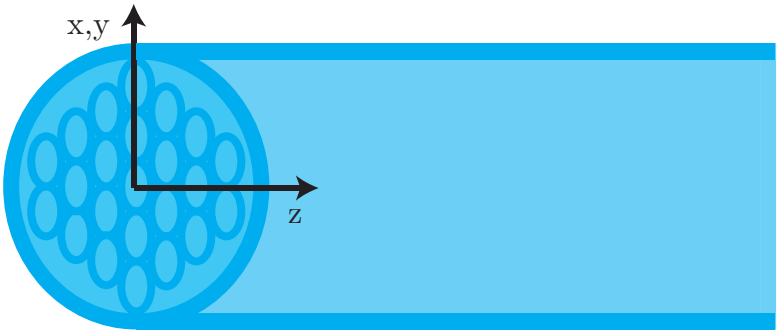

Figure 12: Example for a photonic crystal fiber consisting of an array of glass rods

distance is indistinguishable compared to the unshifted system. In the particular case of a photonic crystal fiber it means that any cross section along the fiber is equivalent. The translation symmetry is described by a translation operator $T_{\vec{d}}$ acting on a function $T_{\vec{d}} f(\vec{r}) = f(\vec{r} - \vec{d})$ with the vector $\vec{d}$ along the direction of the symmetry, for example the dielectric function of a crystal with a continuous translation symmetry along the

[7] neglecting the core as a defect

z-axis $T_{d\vec{e}_z}\varepsilon(z) = \varepsilon(z-d) = \varepsilon(z)$. Such a fiber may look like the fiber in figure 12. As this operator describes the symmetry of the system it commutes with the master operator Θ. For a plane wave the eigenvalue equation for the translation operator is $T_{d\vec{e}_z}e^{ikz} = e^{ik(z-d)} = e^{-ikd}e^{ikz}$ and the eigenvalue is e^{-ikd}. One can proof that in case of a continuous translation symmetry along the z-direction all eigenmodes have the functional form

$$\vec{H}_{k_z}(\vec{r}) = e^{ik_z z}\vec{h}(x,y)$$

so they are proportional to a plane wave propagating along the z-axis with a certain wavevector k_z. In other words the wavevector component along the symmetry axis is conserved [35].

A discrete translation symmetry describes a system which is invariant under a translation of a certain length, the lattice constant. For example, in figure 12 is a discrete periodicity along the y-axes, with the lattice constant b the distance between two rods. The dielectric function is periodic $\varepsilon(\vec{r}+l\vec{b}) = \varepsilon(\vec{r})$ where l is an integer multiple and $\vec{b} = b\vec{e}_y$ the lattice vector along the symmetry axis. The volume of the dielectric that is repeated to provide the periodic structure is called unit cell. The translation operator $T_{l\vec{b}}$ describing the symmetry is commuting with the master operator. It has plain waves as eigenfunctions $T_{l\vec{b}}e^{-ik_y y} = e^{ik_y(y-lb)} = e^{-ik_y lb}e^{ik_y y}$. One hast to note that not all values of k_y lead to different eigenvalues. All values $k_y + l\frac{2\pi}{b}$ with l an integer number lead to the same eigenvalue. Any linear combination of those eigenfunctions is again an eigenfunction, therefore we can expand the modes of the photonic crystal in plane waves

$$\begin{aligned}\vec{H}_{k_y}(\vec{r}) &\propto \sum_l \vec{c}_{k_y,l}e^{i(k_y+lb)y} \\ &= e^{ik_y y}\sum_l \vec{c}_{k_y,l}e^{ilby} \\ &= e^{ik_y y}\vec{u}_{k_y}(y).\end{aligned} \tag{24}$$

The discrete translation symmetry allows us, again, to characterize the modes of a photonic crystal, namely with the wavevector along the symmetry axis. Equation 24 is know as Bloch-Floquet theorem which states that a eigenfunction of a periodic system can be written in a product of a periodic function and a plane wave. Here $\vec{u}_{k_y}(y)$ is by construction a periodic function, which can also depend on the other coordinates and $c_{k_y,l}$ are expansion coefficients. The periodic function is also known as Blochmode. A Blochmode for a given wavevector k_y and all other Blochmodes with the wavevectors $k_y + l\frac{2\pi}{b}$ represent the same physical state. Also the frequencies $\omega(k_y) = \omega(k_y + l\frac{2\pi}{b})$ are the same. This simplifies the problem to wavevectors from the interval $-l\frac{2\pi}{b} < k_y \leq l\frac{2\pi}{b}$, the Brillouin zone.

In the case of a photonic crystal fiber with a continuous translation symmetry along the fiber axis and a discrete translational symmetry in x,y direction we can classify the modes of the fiber with the transversal and the axial wavevector.

To find the modes a photonic crystal supports one has to solve the master equation, see equation 22. Results of calculations are usually presented in bandgap diagrams

which show propagating or evanescent modes for a certain propagation direction and for certain frequencies.

3.3. Bandgap Diagrams

The idea of trapping light in a periodic lattice of microscopic holes in glass was first reported by Russel in 1991 [7]. The first theoretical predictions of a system guiding light in a hollow core were done by Birks et al in 1995 in [6]. They investigated a photonic crystal, namely an array of hexagonal arranged hollow silica rods, similar to the sketch in figure 12. Figure 13 shows the bandgap diagram for the hexagonal array

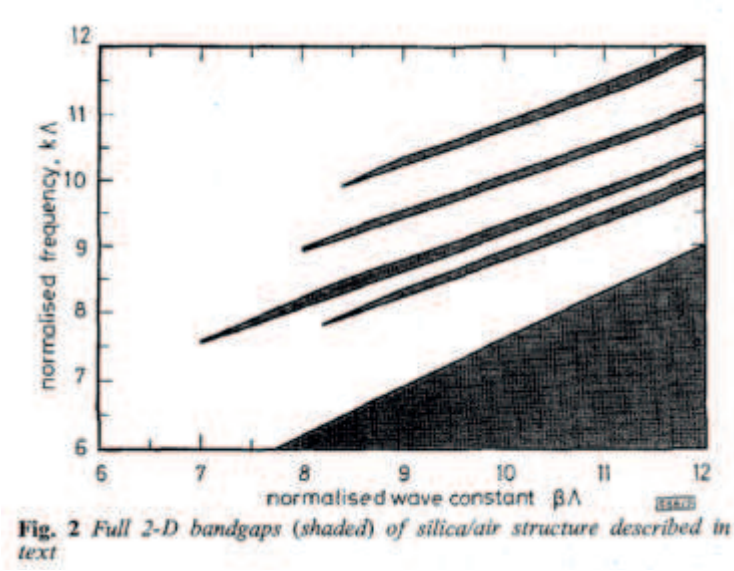

Figure 13: Bandgap diagram for a hexagonal array of circular rods, graph from [6]

of circular rods in a background of fused silica. The spacing of rods is Λ, the vacuum wave constant or frequency is $k = \frac{\omega}{c}$ and β is the wavevector component along the fiber axis. For a given normalized frequency and propagation constant $\Lambda k, \Lambda\beta$, transverse wave vectors for eigenmodes of the photonic crystal are determined. The black areas indicate imaginary transverse wavevectors and the white areas real valued transverse wave vectors. An imaginary wavevector leads to an exponentially decaying, evanescent field meaning light cannot penetrate this direction. The black areas therefore indicate parameters where light cannot propagate in transversal direction.

The semi infinite bandgap on the right bottom part of figure 13 would be expected for any material with refractive index n because at a fixed frequency ω the maximal value β can take is nk, with n the refractive index of the region under consideration. For $\beta < nk$ light is free to propagate. As

$$kn = \sqrt{\beta^2 + (k_\perp)^2}$$

and if $\beta > nk$ this equation does not have a solution and therefore no propagating mode can exist.

There are additional band gaps for lower β values with $\frac{\beta}{k} = n < 1$ less than the index of air, which cannot appear in uniform dielectric materials. Adding any defect in the centre of this structure which breaks the photonic crystal provides a core for the fiber. Any guided mode with a wavevector from the photonic bandgap cannot penetrate the photonic crystal cladding and therefore must be localised in the core.

Figure 14 shows two band gap diagrams, one for a doped SMF and one for a PCF from [7]. The structure of the two fibers is indicated with the inlet on the top left corner of every plot. The PCF has a periodic array of holes and a silica core in the centre. The coloured regions indicate in which part of the fiber light is free to propagate. In the dark blue region (1) it is free to propage in air, silica and the doped core (air, photonic crystal, silica core for the PCF), in the light blue region in silica and the doped core (photonic crystal and silica core for the PCF) and so on. In the black region (4) in both plots is no propagation possible as $\beta > kn$.

For SMF guided modes appear if light is free to propagate in the core and evanescent in the cladding (red strip in figure 14). The underlying guiding mechanism is TIR. There is also a TIR region for the PCF, the yellow region in the band gap diagram (3). On the other hand there are additional black areas indicating full photonic bandgaps in transverse direction providing bandgap guidance. Some of the fingers even range into the region where light is free to propagate in air. This fact provides the possibility for photonic band gap guidance in air, although the refrective index of air is lower than the refractive index of the photonic cladding. The bandgap diagram in figure 13 also shows this feature. There are full two dimensional bandgaps for $\beta/k < 1$.

The novel particle source takes advantage of this fact that light is confined in a small core, which allows optical trapping and transport of nanoparticles.

3.4. Properties

PCF offer advantages compared to standard single mode fibers in particular due to the design that allows to tailor properties as number of guided modes, birefringence, numerical aperture, single mode broadband super continuum or endlessly single mode fiber for all wavelengths. The review [36] gives a deeper inside into PCF.

The guided mode intensity distribution of a HCPCF can be described [8, 37] with

$$I(r,z) = IJ_0^2\Big(2.4\frac{r}{R}\Big)e^{-\alpha z}$$

with J_0 the Bessel function of zeroth order, R the hollow core radius, I the intensity and α the overall loss parameter of the fiber. The overlap with a Gauss mode profile is close to unity. Hollow core fiber losses are cause by similar loss mechanisms as for single mode fibers: Rayleigh scattering, confinement loss, bending loss, absorption, variations in the fiber structure along the axis. This losses might be reduced to lower values than for SMF as scattering and absorption losses are much lower in air than in silica. State of the Art SMF have a loss of 0.2dBm/km which is so far out of reach for HCPCF. The main loss mechanism seems to be surface roughness of the core walls, yet a loss of 3.5dBm/km was reported lately [38].

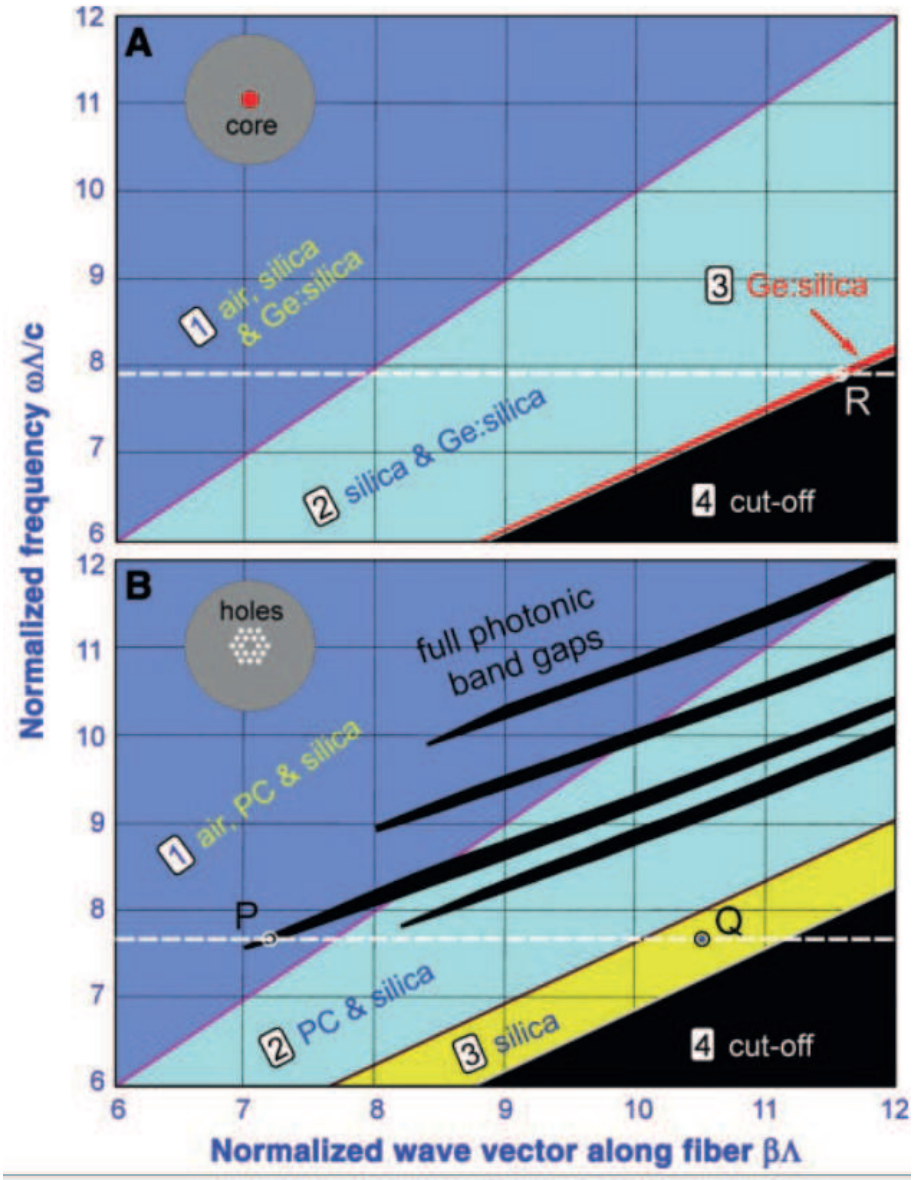

Figure 14: Bandgap diagramm for a doped SMF and a PCF, graph from [7]

4. State of the Art

Guiding particles through a hollow core photonic crystal fiber is not a new idea. First particle guidance experiments using hollow core fibers were done by Renn et al. [39] with atoms. This scheme was expanded to bigger particles in 1998 also by Renn et al. [40]. With continuous improvement and commercial availability of hollow core photonic crystal fibers the number of similar experiments increased. In this chapter will summarize some experiments on guiding particles in HCPCF and results related to this work.

4.1. Leviatation and Guidance of Particles in Air

Most of those experiments have a similar setup consisting of a particle source and one (two) laser beams which are coupled into a hollow core photonic crystal fiber. Particles from a source are brought close to the fiber entrance. The gradient force of a converging laser beam centres particles on axis and the scattering force pushes them towards the fiber. If there is just one laserbeam the particle is then launched into the fiber and propelled through the hollow core. Having a second laser beam, typically orthogonal polarised, entering the other end of the fiber adds a second scattering force pointing in the opposite direction. By changing the power ratio of the two beams it is possible to propel in both directions along the fiber.

The first particle guidance experiment with mesoscopic particles was performed in 1998 by Renn, Pastel and Lewandowski [40]. Hollow core fibers with diameters ranging from 10 to 50μm were used to guide particles between 10nm and 10μm size. They were able to demonstrate guiding of a 7μm polystyrene sphere in a water filled hollow core fiber with a core diameter of 20μm and a laser operating at $\lambda = 800$nm, $P = 240$mW. Also in air filled HCPCF they were able to propel a variety of materials[8] at room pressure with a laserpower $P = 0.5$W. There were two realisations of the setup, the first one with a single laser beam coupled into the hollow core fiber as shown in figure 15 (without piezoelectric source) and a second setup used two laser beams coupled into both fiber ends as shown in figure 16. The range particle were transported is mentioned with several cm. For water droplets, glycerin droplets and the crystals like salt the usage of an nebulizer source is mentioned, no statement about how the other materials were launched.

A second experiment about particle guidance through a HCPCF was reported by Benabid, Knight and Russel in 2002 [8]. Figure 15 shows the setup of the Benabid et al. experiment. They prepared 5μm polystyrene spheres on a microscope cover glass slide attached to a piezoelectric crystal. A green laserbeam (wavelength $\lambda = 514$nm , power $P = 80$mW) is focused through the cover slide into a HCPCF with a core diameter of 20μm. Driving the piezo on resonance (80 kHz) accelerates the particles enough to overcome Van der Waals forces and to leave the cover slide. The free particles were then guided by radiation forces towards the HCPCF, launched into the fiber and transported along. The particle motion was monitored with two CCD cameras detecting

[8] water droplets, glycerin droplets, salt-, sugar-, KI-, CdTe-, Si-, Ge crystals and Au- ,Ag-metal particles of sizes between 50nm and 10μm in a 17μm

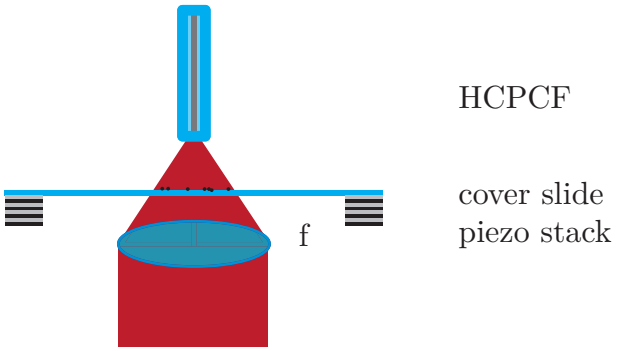

Figure 15: Simplified setup of the Benabid et al. [8] levitation experiment

the scattered light from the particles. Guiding particles through the fiber was possible over a range of almost 150mm with a speed of approximately 1 cm/s at room pressure.

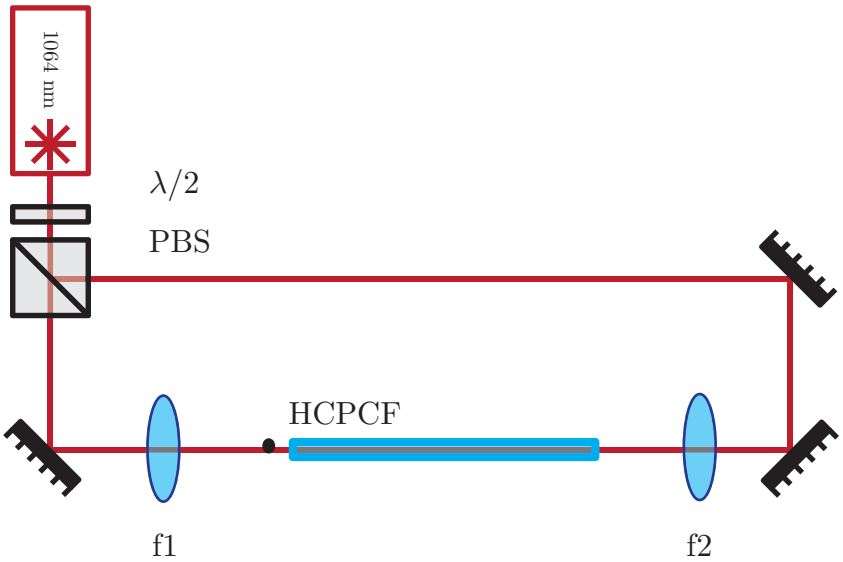

Figure 16: Simplified setup of the Schmidt et al. [9] levitation experiment

Schmidt et al. [9] report trapping and guiding of micrometer sized particles in hollow core fibers and a precise measurement method for the particle velocity and some material properties of the particle. Figure 16 shows a schematic of their setup. A 1064nm laser is split up with a halfwaveplate ($\frac{\lambda}{2}$) and a polarising beam splitter (PBS). The transmitted and the reflected part are coupled into a HCPCF with a core diameter of 12μm. They prepared 5μm particles on a cover slide attached to a piezo and placed it below an entrance of the hollow core fiber. Driving the piezo on resonance accelerates particles enough to overcome Van der Waals forces and to leave the cover slide, as in [41]. An optical trap was provided by a converging beam coupled into the fiber and a diverging beam leaving the fiber. Once a particle is trapped in front of the fiber they were able to move it into the fiber by changing the power ratio between the laser beams.

Transport over distances up to 5m was reported. The particle velocity was measured with a CCD camera and with a in fiber Doppler velocimetry, as in [42]. The scattered light of moving particles and reflected light from the fibre entrance interfere. This interference pattern contains the Doppler shift of the moving particle giving a precise tool to measure its velocity. The velocity measurement and knowledge of the particle radius allows characterisation of density and refractive index of the trapped particle.

In [43], a similar system as Schmidt et al. [9] is used for trapping micrometer sized particles in front of a hollow core fiber. A part of the hollow core fiber is heated which is then used to study photophoretic forces and thermal creep flow in the system.

	core ∅ [μm]	radius a [μm]	transport	source
Renn et al.[40]	10-50	0.01-10	several cm	nebulizer source mentioned
Benabid et al. [8]	20	5	15 cm	piezo
Schmidt et al.[9]	12	5	500 cm	piezo

Figure 17: Summary of the key parameters (HCPCF core diameter, particle radius, range a particle was guided, particle source) of the three mentioned state of the art experiments above

4.2. Trapping of Particles in Liquid filled Hollow Core Photonic Crystal Fiber

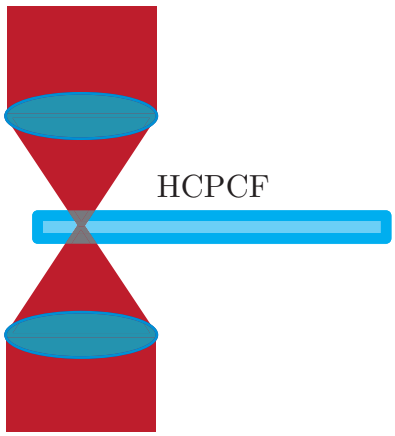

Figure 18: Schematic setup for transverse trapping in HCPCF

Trapping micrometer sized particles in liquid using hollow core fibers was reported in [44] for studying microfluid drag forces and optical and chemical properties of the particle. In [42] a Doppler velocimetry for a particle moving in a liquid filled hollow core fiber has been reported. Several authors [45, 46, 47, 48, 49] report transverse

trapping in hollow core fibers with a system exemplary shown in figure 18. One (or two counterpropagating) laser beams are focused through the photonic crystal cladding trapping a particle in a liquid filled hollow core.

It is worth mentioning that in none of the above reported experiments a standing wave was used, either for trapping or changing the particle position. Despite the Renn et al. experiment [40] no experiments with nanoparticles trapped in an air filled or vacuum environment HCPCF were reported, see summary in figure 17.

We are going to use a standing wave to have additional control over the particle position compared to solely scattering force based methods.

In this context the novel particles source experiment is the first one using HCPCF for optical trapping and transport of nanoparticles into vacuum.

5. Experiment and Methods

This chapter describes the experiment built to realize the novel particle source and the methods which are used to transport and trap nanoparticles with HCPCF.

5.1. Experimental Setup

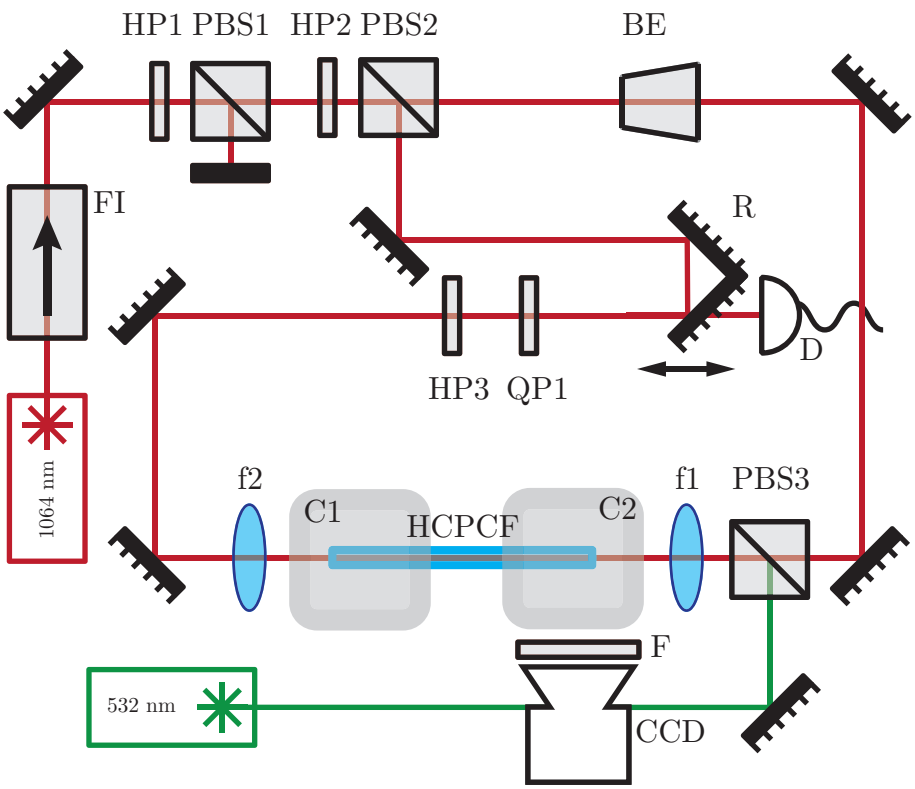

Figure 19: Experimental setup: A infrared laser passes a Faraday Isolator (FI) and is split up into a clockwise (CPB) and a counterclockwise (CCPB) propagating beams with HP2 (half waveplate) and PBS2 (polarizing beam splitter). The overall power can be set with HP1 and PBS1. The CPB passes a beam expander (BE) and is focused into the HCPCF (f1) whereas the CCPB is focused (f2) into the other end of the HCPCF. The CCPB pathlength can be changed with a retro reflector (R) on a translation stage. R transmits roughly 10% of the impinging light on a photodiode (D). HW3 and QP1 (quater waveplate) are set to form a standing wave within the HCPCF. The HCPCF connects loading chamber C1, connected with a nebulizer source, with the science chamber C2. The green beam line is used to excite fluorescent nanoparticles and the camera (CCD) in combination with a Filter (F) to detect them.

Figure 19 shows a simplified version of the experiment. Some polarizing optics for power adjustment are neglected in the drawing for better overview. The vacuum chamber

(C1) is connected with an nebulizer source, as described in chapter 5.2 and with a pump. The vacuum chamber (C2) is only connected with vacuum pumps. One end of a 10 cm long HCPCF is mounted inside the vacuum chamber C1. The other end is mounted in chamber C2. A HCPCF (1060HC from NTKPhotonics) is used in this experiment (figure 11). Modeshape, dispersion, attenuation curve and other properties are listed in the data sheet in Appendix A. The diameter of the hollow core is 10μm, the mode field diameter of the HCPCF is $2\omega_{\mathrm{hc}} = 7.5\mu$m and the loss coefficient is smaller then $\alpha < 0.1\frac{\mathrm{dB}}{\mathrm{m}}$. The vacuum chambers are sealed with epoxy glue at the fiber entrance. A infrared laser (Coherent Verdi IR25, $\lambda = 1064$nm, $P = 25$W, frequency tunable up to $\Delta\nu = 3.2$GHz) first passes a Faraday isolator (FI) to protect the laser from back reflected light, is then attenuated with PBS1 (polarising beam splitter) and a halvwaveplate (HP1) to choose the overall power. It is split up into a clockwise (CPB) and an counterclockwise (CCPB) propagating beam at PBS2. With the halfwaveplate (HP2) in front of PBS2 the power ratio between both arms can be set. The beam size of the CPB is increased at a beam expander (BE) to a waist of $\omega = 3.2$mm, focused with an achromatic lens, focal length f=35mm (f1), into the HCPCF. The waist in the focal point matches the mode field diameter of the HCPCF. The CPB is set to be horizontal polarised.

The CCPB is focused into the HCPCF with an achromatic lens, focal length f=18mm (f2). To guarantee that both beams have the same polarisation and form a standing wave, a halfwaveplate (HP3) and a quarterwaveplate (QP1) in the CCPB path can be aligned accordingly. The two waveplates are optimized to have a minimum in the reflected port at PBS3.

In the CCPB arm is a retro reflector (R) mounted on a translation stage which can change the pathlength of the CCBP. One of the mirrors in R is a 90:10 beamsplitter transmitting 10% of the CPB onto a photodiode (D) which is used for position read out of the particle motion.

The second beam line with a green laser pointer ($\lambda = 532$nm, $P \approx 25$mW) has been used to excite fluorescent nanoparticles. The HCPCF tip was expected to scatter much more light as a particle trapped in front. Fluorescence offered an easy way to separate scattered light from a particle and the trap. The green laser is superimposed with the infrared at PBS3 and focused (f1) into the HCPCF. The HCPCF does not support green light but a particle trapped in front of the fiber can be excited. After realizing that non-fluorescent particles can also be imaged, this part of the experiment was disabled.

A combination of a camera (CCD, Playstation Eye, infrared filter removed), a fluorescent filter (F) and an achromatic lens with a focal length $f = 30$mm (not shown in figure 19) images the front part of the HCPCF located inside the vacuum chamber. The filter matches the emission spectrum of the fluorescent particles and suppresses 1064nm light scattered from the fiber tip. For non-fluorescent particles the filter F is replaced with a hot mirror suppressing roughly 95% of the impinging 1064nm light.

5.2. Evaporative Source and Particle Preparation

The experiment is performed with two different species of nanoparticles. First, 190nm diameter fluorescent polystyrene spheres (FS02F/10353, Bangs Laboratories Inc.) were

used. They can be excited with green light and have their emission maxima around 610nm. The second species are $a = 127$nm radius plain silica spheres (microspheres-nanospheres.com). Loading particles was done similar to [11]. Both types of particles are delivered in aquatic solution with a mass concentration of 10 %. It is diluted with Isopropanol to a mass concentration of 0.1‰ and kept for approximately 10min in an ultrasonic bath. To get the particles airborne the solution is nebulized with a medical asthma spry (Omron MicroAir) into mist with a maximum droplet size of 3 μm, see also McGloin [12]. The asthma spray is in a closed box which is connected with 1m long and 6mm thick steel tube to the vacuum chamber. Mounted in between is a valve to regulate the flow into the chamber and a diffusion dryer (Livermore Instruments). This is a 30cm long tube filled with activated charlcoal which filters alcohols from the air passing through. Isopropanol evaporates quickly after spraying and in combination with the Diffusion Dryer this loading mechanism should provide a stream of airborne nanoparticles. By opening the valve particles will float into the vacuum chamber and get eventually caught in the optical trap.

5.3. Optical Trap

CPB and CCPB have equal polarisation and are focused into a HCPCF forming a standing wave as described in chapter 2.2. The mode profile inside the HCPCF can be approximated with a TEM00, see chapter 3.4. The trap depth is constant within the HCPCF because waist and power do not change. The trap potential inside the HCPCF is described by equation 7 with $\omega(z) = \omega_0$. The waist after the HCPCF is not constant any more $\omega(z) = \omega_0\sqrt{1 + \left(\frac{z}{z_R}\right)^2}$ and therefore the trap depth decreases further away from the fiber end (at $z = 0$). There will be a range where trapping in front of the HCPCF is still possible depending on the trap depth. Light is coupled into the HCPCF with efficiencies between 50% and 70%, depending on the quality of the cleave, see Appendix B. The attenuation for 1064nm light in the fiber is specified with $0.1\frac{\mathrm{db}}{\mathrm{m}}$ and is therefore negligible for a 10cm long piece of fiber. Optical trapping and particle transport was typically done with 2W (or 1.5W) optical power in the CPB and CCPB, always measured in transmission of the HCPCF. The calculated trap depth is then 2.5×10^6K (or 2×10^6K) inside the HCPCF for a 127nm silica particle (equation 7). The kinetic energy of a thermalized particle is $k_B T$ at room temperature (T=300K) and therefore 830 (660) times smaller than the trap depth. The radial root mean square displacement by a thermal 127nm silica particle is then rms $= \sqrt{\frac{2k_\mathrm{B}T}{m\Omega^2}} \approx 120$nm (140nm), much smaller than the HCPCF core.

Figure 20 shows the trap depth in the HCPCF trap in dependence on the particle size with an optical power of 1.5 W.

Particles are trapped in the following steps. First, the two beams are aligned with sufficient power to the HCPCF. Secondly the loading chamber is pumped below 100mBar to be able to suck nanoparticles from the nebulizer through the tube into the chamber. The valve in between is then carefully opened letting particles flow into the loading chamber. In order to capture particles it is necessary to let the pressure in the chamber

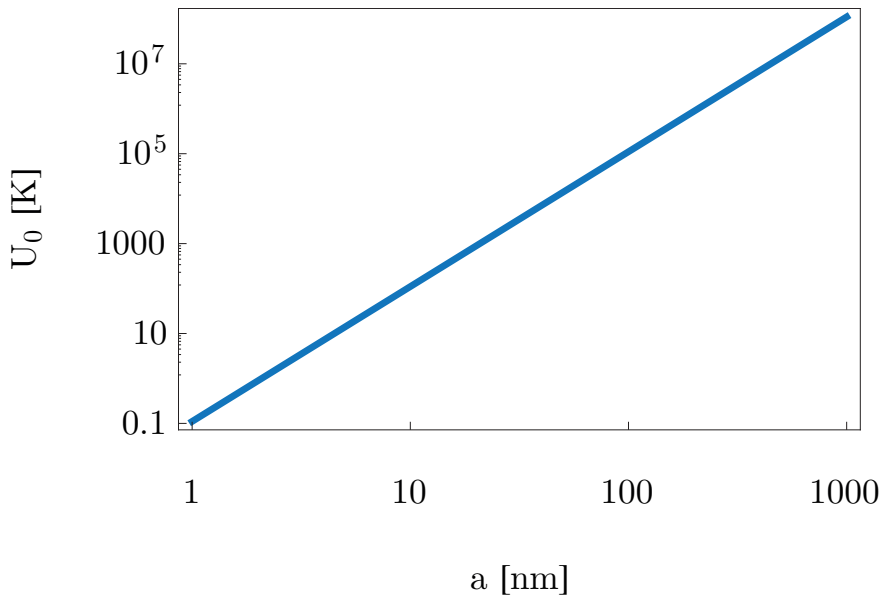

Figure 20: Trap depth U_0 of a standing wave with 1.5 W optical power for silica spheres depending on the radius a

equilibrate with room pressure. After closing the valve and waiting a few seconds a particle will be trapped in front of the HCPCF.

5.4. Moving Mechanisms

As soon as a particle is trapped in front of a HCPCF there are several ways to change its position.

5.4.1. Particle Propelling

One beam can be blocked in order to harness the scattering force F_{scatt} from the other beam to accelerate the particle. The final velocity of the particle depends on the scattering force and the drag force within the HCPCF. The equation of motion is

$$\ddot{z} = -\gamma \dot{z} + \frac{F_{\text{scatt}}}{m} \tag{25}$$

where the scattering force is constant over the entire fiber length and γ the damping rate (equation 10). The solution of equation 25 is $x(t) = \frac{F_{\text{scatt}} t}{\gamma} - \frac{e^{-\gamma t}}{\gamma} c_1 + c_2$ with c_1, c_2 the initial conditions. For an initially resting particle the velocity is $v(t) = \frac{F_{\text{scatt}}}{\gamma}\left(1 - e^{-\gamma t}\right)$. The inverse damping rate γ is telling how fast the particle reaches its final velocity $v_\infty = \lim_{t\to\infty} v(t)$. Figure 21 shows the velocity of a 127nm silica particle at room pressure (blue curve) and at 100mbar (red curve) for an optical power of 1.5W.

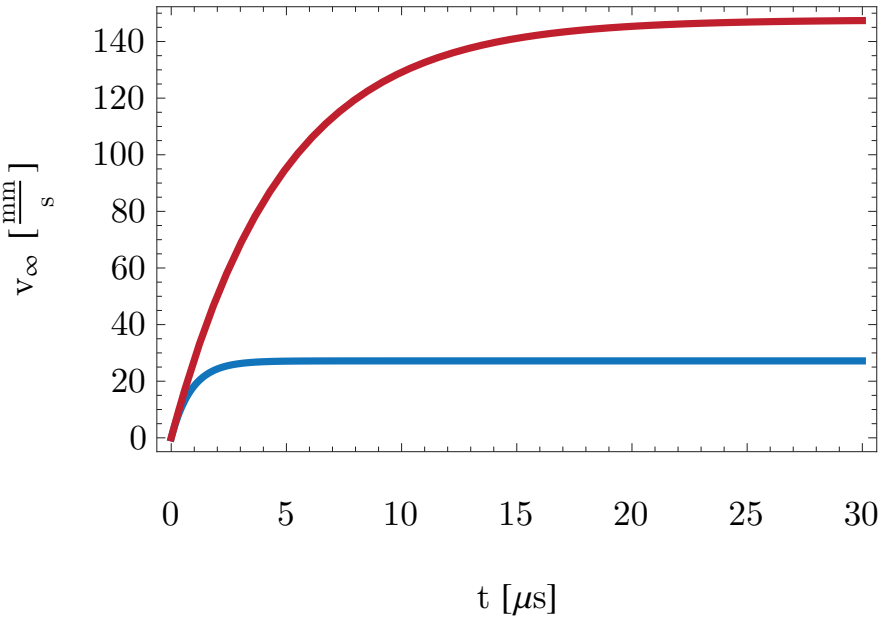

Figure 21: Velocity of a 127nm silica particle in a HCPCF accelerated by the scattering of one beam with 1.5 W optical power at room pressure (blue curve) and at $p = 100$mBar (red curve)

5.4.2. Particle Motion due to an overall Frequency Change

Another way to change the particle position can be implemented via an overall frequency change of the laser. PBS2 in figure 19 splits the laser into two counterpropagating beams where one roundtrip has the optical length L. The light field at any position z within the roundtrip is the superposition of the CPB and the CCPB beam

$$\begin{aligned} I(z) &\propto \left|e^{ikz} + e^{-ik(z-L)}\right|^2 \\ &= \left|e^{ik(z-\frac{L}{2})} + e^{-ik(z-\frac{L}{2})}\right|^2 \\ &= 4\cos^2\left[k(z-\frac{L}{2})\right]. \end{aligned}$$

At half the optical path length $\frac{L}{2}$ is always an intensity minimum $I(z = \frac{L}{2}) = 0$ independent of the laser frequency.

A particle is trapped in an intensity maximum, where $\cos^2(kz) = 1$ such that the particle position z is always a multiple of half the wavelength $z = n\frac{\lambda}{2}$. Changing the wavelength of the laser from λ to $\lambda' = \lambda + \Delta\lambda$ changes the particle position to $z' = n\frac{\lambda'}{2}$ as it stays in the same intensity maximum. The position change of a trapped particle

in a standing wave induced by a frequency change is therefore

$$d(z, \Delta\nu) = \frac{\partial z'}{\partial \lambda}\Delta\lambda = \frac{n}{2}\Delta\lambda \tag{26}$$

$$\approx z\frac{\Delta\lambda}{\lambda} = z\frac{\Delta\nu}{\nu}. \tag{27}$$

Figure 22 sketches the mechanism. The red line is a standing wave with a trapped nanosphere (indicated by a dotted circle). Changing the laser frequency moves the intensity maxima closer together (blue line) and therefore the nanoparticle (black circle) closer to the intensity minimum $\frac{\lambda}{2}$.

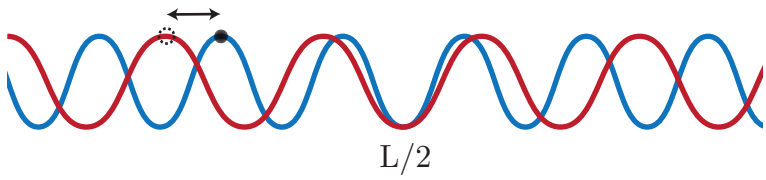

Figure 22: A particle (dotted circle) is trapped in a standing wave (red line), an overall frequency change squeezes the maxima closer together (blue line) and changes the particle position (black circle)

Laser frequency noise will lead to modulations of the particle position. In this setup the Verdi IR25 is specified with a linewidth of $\delta\Delta\nu = 2.5$MHz causing a position uncertainty due to laser noise $\Delta d(z, \nu) = z\frac{\delta\Delta\nu}{\nu} \approx 5$nm at a particle position $z = 0.55$m which is less than the root mean square displacement rms ≈ 6nm of the thermal motion of a particle in axial direction with a radius $a = 127$nm.

5.4.3. Particle Motion due to Displacement of the Standing Wave

The counter propagating beams build a standing wave for equal powers and polarisations where the scattering forces cancel. A particle will always be trapped in a particular intensity maximum. Moving the whole standing wave also moves the particle trapped in this particular intensity maximum.

A simple and effective mechanism to move the standing wave is implemented in this setup. Two mirrors perpendicular to each other form a retro reflector (R, figure 19), mounted on a translation stage. By moving the stage about a distance l the length of one roundtrip is increased by $2l$. The number of maxima between the particle and the intensity minimum at $\frac{L}{2}$ is conserved and so is the distance between the particle and $\frac{L}{2}$. The new length of the roundtrip after moving the stage is $L_n = L + 2l$. The old centre position $\frac{L}{2}$ and the new centre position $\frac{L_n}{2}$ differ by l. As the difference between this position and the particle is conserved and the particle stays always in the same intensity maximum the particle also moves by l.

Another implementation of this transport mechanism can be done by changing the frequency of one of the two counter propagating beams. The standing wave is no longer

stationary, it moves with a certain velocity depending on the frequency difference between CPB and CCPB as in [50] which is called optical conveyor belt.

5.5. Position Read Out

The read out of the particle oscillation is based on the scheme explained in chapter 2.6. In this setup, only the particle motion along the z-direction is monitored. Two different cases have to be considered.

First, a particle trapped in front of the HCPCF leads to the signal calculated in equation 16. The CPB gathers a Gouy phase of $-i\frac{\pi}{2}$ between trap position and detector (D) whereas the dipole radiation of the trapped particle contains a phase depending on its displacement. The part of the CPB which is not affected by the trapped particle acts as a phase reference with which the phase shifted scattered light from a displaced particle can be measured. This signal is separated from the CCPB at R (figure 19), then gathered on D and evaluated with a spectrum analyser.

Secondly, the phase relation between scattered light from a dipole inside the HCPCF and the phase reference beam is expected to be different. Far away from the dipole its emission is in the HCPCF mode as the HCPCF is a mode filter for the dipole scatterer. The additional phase ϕ_D the dipole radiation gathered in the filtering process determines the interference signal measured on D and is unknown so far.

6. Disscussion and Results

In this chapter the different procedures discussed before have been realized with the experiment presented in figure 19.

6.1. Trapping

The very first result was trapping of a fluorescent polystyrene sphere with a radius $a = 95$nm in front of a HCPCF. The particle was excited with the green beam line, described in chapter 5. Capturing was just possible at room pressure, but after trapping pumping down to approximately 10 mbar was possible. For lower pressures the particle was lost.

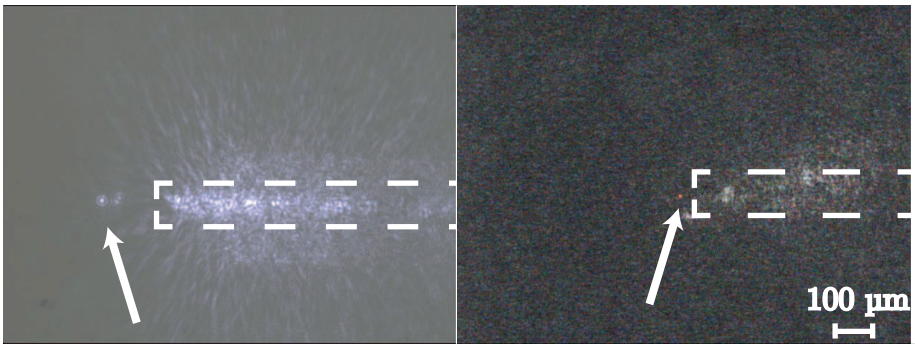

Figure 23: Two 95nm silica particles (arrows) trapped in front of a HCPCF (indicated by the dashed line)

Figures 23 show fluorescent particles trapped in front of a HCPCF. The particle in the right figures scatters red fluorescent light, while the particle in the left figure seems to scatter (for some unknown reason) more infrared light which appears white on the image. As we could observe particles using light at 1064nm despite of bacground scattering from the HCPCF tip plain silica spheres with $a = 127$nm (and $a = 580$nm) where trapped under the same conditions as for the polystyrene spheres. Instead of a fluorescence filter in front of the CCD an attenuator was used.

Capturing particles required at least 1.5 W optical power from both sides, but the minimal power required was not investigated. Although the trap depth provided by 1.0 W of optical power should be sufficient to trap a 127nm silica particle ($U_0 = 1.5 \times 10^5 K$) it did not work. By just increasing the power to 1.5 W and capturing particles again, misalignment could be ruled out as a reason. The thermal energy at room temperature (300K) cannot be the only contribution to the kinetic energy of the particle which has to overcome the trap depth to make a particle escape. It seems that other effects due to the high damping at room pressure dominate the kinetic energy of the particle.

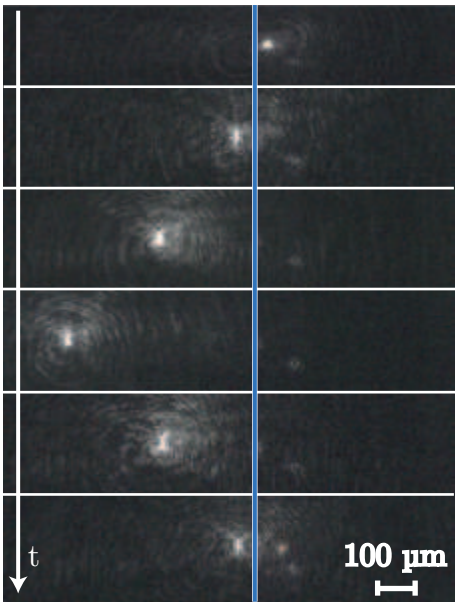

Figure 24: 6 sequential pictures of a 95nm fluorescent polystyrene particle transported inside a HCPCF (fiber entrance indicated by the vertical blue line), removed and held again in front of the HCPCF

6.2. Particle Transport

Particles transport has been demonstrated with different mechanisms, see chapter 5.4. After trapping a particle in front of the HCPCF the particle was shifted into the fiber and taken out again by moving the standing wave with the retro reflector and the stage. Figure 24 shows 6 pictures of a 127nm silica particle moving inside a HCPCF (fiber entrance indicated by the vertical blue line) at room pressure. The particle was transported to the end of the field of view and back out again. Particle transport up to 2.5cm was achieved by this method only limited by the range of the linear stage.

After succesfully moving a particle into the HCPCF blocking the CCPB propelled a particle along the fiber as the scattering force of the CPB accelerates the particle. With this method particles could be moved over the whole fiber length, 10cm in this particular case. By unblocking the CCPB the particle immediately stopped. Figure 25 show pictures of a CCD camera before and after blocking the beam. A shutter with an opening and closing time of 100ms is used for blocking. The distance between the first and the second arrow in figure 25 is approximately 27mm and 22mm between the second and the third arrow. The velocities are then $270\frac{\mathrm{mm}}{\mathrm{s}}$ and $220\frac{\mathrm{mm}}{\mathrm{s}}$. The pressure in the region where the particles were moved is expected to between 1000 and 700mbar (figure 29). Given an optical power of 1.5 W in the CPB, a 127nm particle is expected to have a 10× smaller final velocity, see chapter 5.4. Thus we can only assume that a larger particle or a small cluster of particles has been transported. From the measured velocity and the optical power used the radius of the nanoparticle is expected to be around 200nm (chapter 5.4).

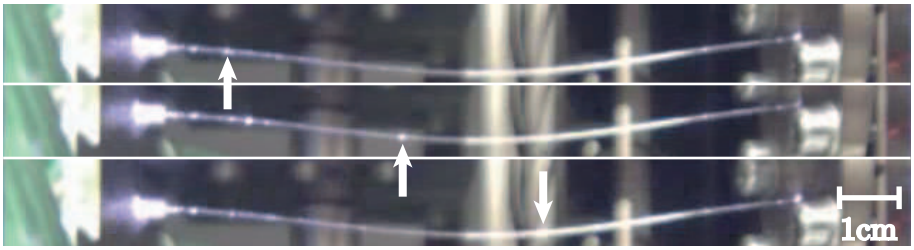

Figure 25: Three sequential pictures of a particle (arrow) pushed through a HCPCF by the scattering force ($P = 1.5$W) of the CCPB while the CPB was blocked with a shutter for 100ms. Each picture shows the particle after one shuttering cycle

Position change by an overall detuning of the laser frequency can be used as a precise particle positioning tool. Figure 26 shows the maximal displacement achievable for a

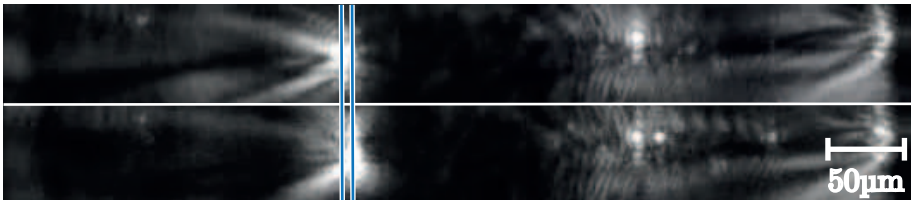

Figure 26: A 127nm silica sphere trapped inside the HCPCF at two different positions (vertical blue lines indicate the centre of the trapped sphere in the first and second picture). A frequency detuning $\Delta\nu = 3.2$ GHz of the standing wave displaces the nanosphere

particle trapped at $z = 0.55$, measured from $\frac{L}{2}$, as explained in chapter 5.4. The top picture is before and the bottom picture after the frequency change. The displacement extracted from the CCD camera is $d = 7 \pm 2\mu$m which agrees with the expected value $d = z\frac{\Delta\nu}{\nu} = 5.7\mu$m for a detuning $\Delta\nu = 3.2$GHz.

All three moving mechanisms have been demonstrated at room pressure (or slightly lower) in science (C2) and loading chamber (C1).

6.3. Position Readout

Figure 27 shows noise-power spectra (NPS), measured as described in chapter 5.5, of a trapped nanoparticle in front of and in the HCPCF.

The blue curve shows the NPS of a trapped 127nm silica sphere in front of and the red curve inside (approximately 1mm) a HCPCF. The mechanical frequency of the particle in front is expected to be smaller as inside because the intensity is lower before the HCPCF. The green curve is the corresponding background signal, a NPS taken with the same experimental parameters but without trapped particle. It contains laser and electronics noise and will be subtracted from the particle NPS to reduce the overall noise level. Fitting the subtracted spectrum of the particle in front the fiber to equation

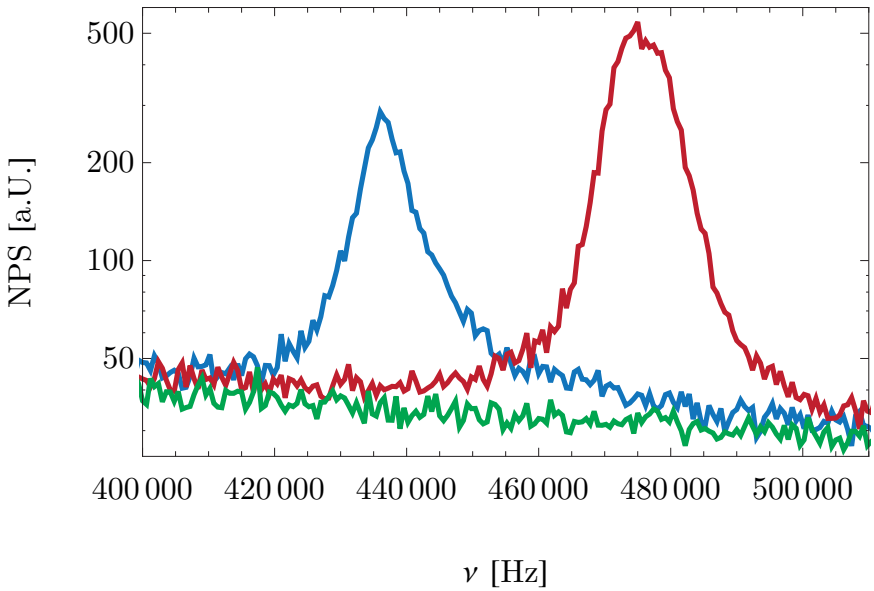

Figure 27: Noise-Power Spectrum of a trapped 127nm silica particle in front of a HCPCF (blue curve), inside a HCPCF (red curve) and a background noise power spectrum without particle (green curve)

13 gives the mechanical frequency and damping rate of the system. As pointed out in chapter 5.5 the phase relation between scattered light from the particle inside a HCPCF and the CPB is not yet known to us. However a signal from a trapped nanoparticle inside a HCPCF can be measured and be related to the particle motion.

The position read out is then used to test the frequency-power dependence of the optical trap. A 127nm silica particle is trapped in front of the HCPCF and the power of both arms was simultaneously changed using HP1 and PBS1 (figure 19). First, a NPS with particle is taken for each power and later a NPS without particle for each power. The mechanical frequency from the subtracted NPS is plotted against a power P_D proportional to the power in the trap in figure 28. It is measured in transmission of the 90:10 beamsplitter in R from the CCPB. The blue curve is a fit of $f(P) = const\sqrt{P}$ to the measured data, as the mechanical frequency is proportional to the square root of power (equation 9). The free fit parameter *const* covers the material properties and the conversion factor from the measured power to the power in the trap.

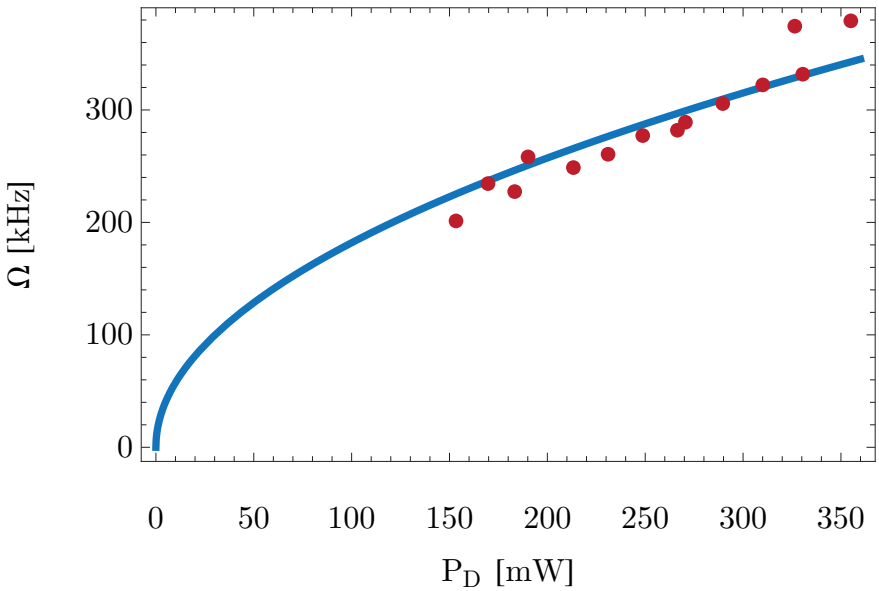

Figure 28: Frequency power measurement of a trapped nanoparticle in front of the HCPCF. The mechanical frequency is plotted against optical power P_D proportional to the power in the trap (red dots) and a square root function in power is fitted (blue curve)

7. Conclusions and Outlook

The aim of this thesis was to build a novel particle source, an experiment capable of transporting nanoparticles from a nebulizer source to a desired place in a science chamber, compatible with UHV experiments. Trapping nanoparticles of the desired size, especially 127nm which are used in [11], in front of a HCPCF and transporting it inside a HCPCF was shown. Three different moving mechanisms (chapter 5.4) to transport particles were successfully demonstrated at room pressure. Also position readout of the motion is implemented.

Those three different moving mechanisms in combination allow a particle transport over arbitrary distances with high precision, better than the thermal motion of the particle. By blocking the CCPB long distances over the whole HCPCF length can be, in principle, covered and was shown for 10cm. The particle was stopped, by unblocking the CCPB, within 2.5cm distance to the desired end position, which can then be overcome by moving the particle with the stage and the retroreflector (R, figure 19). A final high precision alignment of maximal 5μm can be achieved by laser detuning only limited by laser noise which leads to a position inaccuracy of 5nm.

This setup provides now two of the three required features of the introduction. A particle source which allows transport of nanoparticles from a separated loading chamber, containing a nebulizer source, into a clean science chamber without contamination at a defined place is possible. Secondly it allows control over the amount of nanoparticles delivered into the science chamber.

To realize the third requirement, loading at UHV conditions, two further aspects has to be considered.

First, it was shown that the HCPCF can overcome nine orders of magnitude in pressure from loading chamber to science chamber. Adding an intermediate chamber to the source allows to bridge even more orders of magnitude. Therefore this system provides the pressure requirements for an UHV experiment.

The second aspect is more crucial and not investigated in this thesis. Other experiments report loosing particles in an optical trap below approximately 1 mbar [11, 13] for yet unknown reasons. It is likely that the HCPCF trap will face the same problems. It is interesting to know where this critical pressure occurs in the HCPCF. There is few work done on pressure distributions in small tubes connecting a high pressure reservoir with a low pressure reservoir. The only publication know to the author providing an experimentally verified theory (from room pressure down to 5mbar) is [24]. Based on their calculations figure 29 shows the pressure distribution along a 10cm long tube with a core diameter of 10μm. It is connected with a high pressure reservoir (1000mbar) on one end and a low pressure reservoir (220mbar) on the other. One of their claims is that the theory also holds true for lower pressures. The inset shows a pressure distribution for the same tube but connected with a low pressure reservoir at 10^{-7}mbar. If this distribution holds true the pressure drops from 10mbar, a pressure where trapping should still be possible, to the low pressure of 10^{-7}mbar in the last 100μm in the HCPCF. Therefore it is worth continuing the approach started in this thesis. One could think of building the HCPCF source in a vertical arrangement, transport a nanoparticle close to

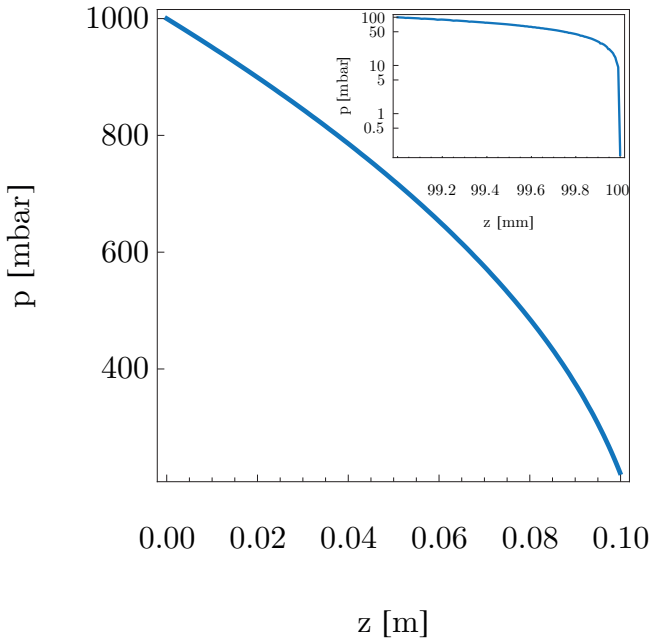

Figure 29: Pressure distribution along a 10cm long tube with a core diameter of 10μm connected with a high pressure reservoir (1000mbar) and a low pressure reservoir (220mbar). The inset shows the pressure distribution between room pressure and 10^{-7}mbar, based on calculations from [24]

the fiber end where the critical pressure occurs, switch the light off and let the particle fall due to gravity into an experiment below the HCPCF.

On the way there the pressure distribution along the fiber predicted by [24] can be tested as this experiment can measure damping rates and therefore the pressure on any position in the HCPCF.

Last and most important as promising results were achieved in terms of position control, particle number control, non-contamination and the outlook of UHV compatibility our experiment on cavity cooling of levitated nanospheres [11] will be equipped with this source.

A. HC-1060 Data Sheet

NKT Photonics
the power of light

Crystal Fibre • *aero*LASE • Koheras • SuperK

HC-1060-02

Hollow Core · Spectral Filtering

Hollow Core Photonic Bandgap Fiber for 1060nm Range Applications

- >95% of optical power located in air
- Quasi-Gaussian fundamental mode
- Can be filled with gas
- Low bend loss down to few mm bend radius
- Fresnel reflection to air at the end faces <10^{-4}
- Up to 80% of fiber cross section composed of solid silica, facilitating fusion splicing to conventional fibers
- Undoped silica for good temperature stability

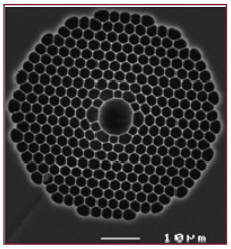

Hollow core photonic bandgap fibers guide light in a hollow core surrounded by a microstructured cladding formed by a periodic arrangement of air holes in silica.

Since only a small fraction of light propagates in glass, the effect of material nonlinearities is significantly reduced and the fibers do not suffer from the same loss limitations as fibers made from all solid material.

Applications include power delivery, pulse shaping and compression, sensors and nonlinear optics.

Physical properties	
Core diameter*	10 µm ± 1 µm
Pitch	2.75 µm
Air filling fraction PBG region	> 90%
Diameter of holey region	50 µm
Cladding diameter	123 µm ± 5 µm
Coating diameter (single layer acrylate)	220 µm ± 50 µm

Optical properties	
Center wavelength	1060 nm
Attenuation @ 1060 nm	< 0.1 dB/m
Dispersion @ 1060 nm	120 ps/nm/km
Dispersion slope @ 1060 nm	1 ps/nm^2/km
Dispersion slope @ zero disp. wavelength	4.4 ps/nm^2/km
10 dB width of transmission band	> 90 nm
Fraction of light in air	> 90%
Mode field diameter (1/e^2)	7.5 µm ± 1 µm
Effective mode index	~0.99
Mode shape overlap with std. SMF	> 90%

Typical attenuation and dispersion

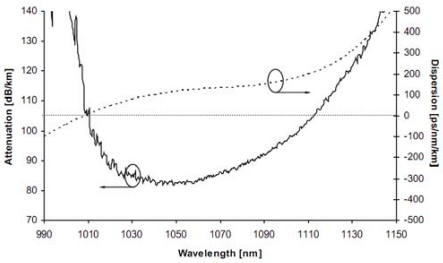

Typical near field intensity

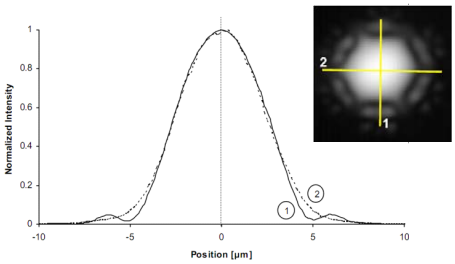

** Core formed by removing 7 hexagonal unit cells of the cladding*

HC-1060-02-100409

NKT Photonics A/S (Headquarters)
Blokken 84 • 3460 Birkerød • Denmark
Phone: +45 4348 3900
Fax: +45 4348 3901
www.nktphotonics.com

NKT Photonics GmbH
Schanzenstrasse 39 • Bldg D9-D13
51063 Cologne • Germany
Phone: +49 221 99511-0
Fax: +49 221 99511-650

NKT Photonics Inc.
1400 Campus Drive West • Morganville
NJ 07751 • USA
Phone: +1 732 972 9937
Fax: +1 732 414 4094

B. HCPCF Cleaving

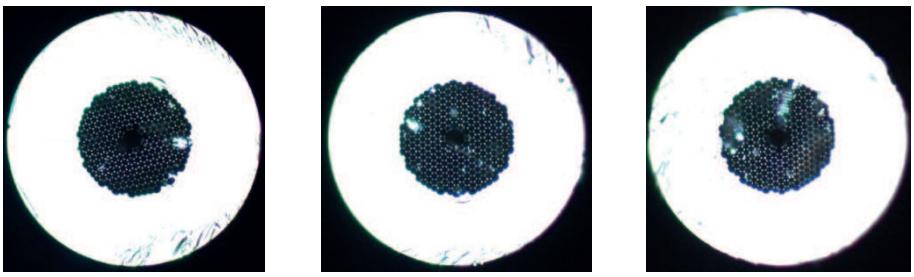

Figure 30: Three different cleaves with a Fujikura CT-30

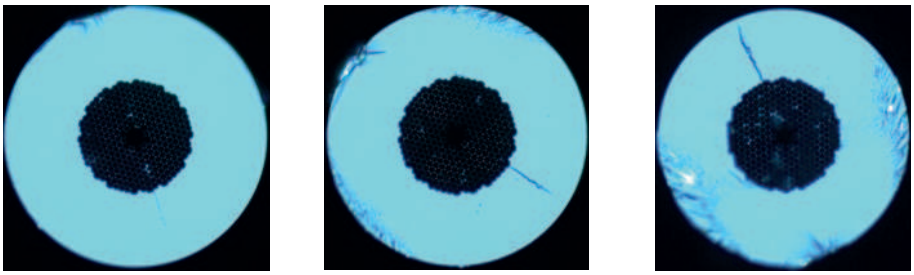

Figure 31: Three different cleaves with a VF-15-H

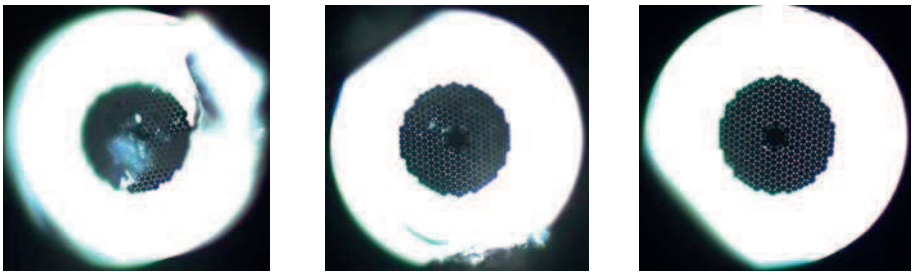

Figure 32: Three different cleaves done manually with decreasing tension on fiber ends (from high tension left picture to no tension right picture)

One crucial parameter to maximise the coupling of light into a HCPCF is the quality of the cleave. From my personal experience it is not as straight forward as cleaving a SMF. I tested two different cleavers from different companies (Fujikura CT-30 and VF-15H) which did not produce sufficiently good results. A cleave is called good if the surface and the photonic crystal is smooth and without bumps. The ambition is having a cleave as shown in the data sheet of the HC1060 (Appendix A). Figure 30 shows three different cleaves from a Fujikura CT-30. The silica cladding looks ok but there are a lot of bumps in the photonic crystal cladding. Figure 31 shows three different cleaves done with a VF-15H. The silica cladding looks worse compared with the Fujikura cleaves but the photnic crystal cladding is smoother. Figure 32 shows three different cleaves done

by hand. First, they were carved with a fiber scribe and than manually cracked. The differences in the cleaving quality depends on the tension applied on the fiber during cracking. From left high tension to right no tension at all. The quality of the cleave on the right side in figure 32 without tension was the best achievable. A flat and smooth silica and photonic crystal cladding. This cleaving result is repeatable with the described procedure.

C. Zusammenfassung

Mit Licht gefangene, kleine Kügelchen in Ultrahochvakuum gewinnen an Aufmerksamkeit als optomechanisches System für Tests von fundamentalen Fragen der Physik [1, 2, 3, 4, 5]. Eine der Herausforderungen solcher Experimente ist die Präparation von nanometer großen Teilchen im Ultrahochvakuum.

Vorgeschlagene Teichengrößen liegen typischerweise um 100nm. Die beiden üblichen Methoden zur Präparation sind ungeeignet. Abschütteln kleiner Teilchen von piezoelektrischen Kristallen ist durch Van der Waals Kräfte limitiert. Der Zugang basierend auf Nanoteilchen in Flüssigkeitstropfen ist schädlich für ein Ultrahochvakuum.

Diese Arbeit stellt eine neue Teilchenquelle vor die optisches fangen mit photonischen Hohlkristalllichtleitern kombiniert. Der Hohllichtleiter hat ein Loch von 10μm mit dem man eine Verneblungsquelle mit einer Experimentenkammer verbinden kann. Eine optische Falle durch den Lichtleiter ermöglicht das Fangen eines Teilchens von der Verneblungsquelle und einen kontrollierten Transport durch den Lichtleiter in die Experimentenkammer.

Das durchgeführte Experiment demonstriert die grundlegenden Funktionsprinzipien des Transports von Nanoteilchen einer Verneblungsquelle durch einen photonischen Hohlkristalllichtleiter in eine Experimentenkammer bei Raumdruck. Der Aufbau erlaubt hohe Positioniergenauigkeit und Charakterisierung der Dynamik von Nanoteilchen. Es wurde gezeigt, dass das System kompatibel mit einer Ultrahochvakuumumgebung ist. Des Weiteren ist das System vielversprechend den Transport eines Nanoteilchen in Ultrahochvakuum zu ermöglichen.

D. Curriculm Vitae

David Grass
(14.03.1987, Neunkirchen Saar, Germany)

Education

1997 - 2006	Illtalgymnasium Illingen, Germany Degree: Abitur
2007 - 2009	Universität Kaiserslautern, Germany Studies in Physics, Degree: Vordiplom
2009 - 2010	Universität Wien, Austria Studies in Physics, Degree: Bachelor of Science
since 2010	Universität Wien, Austria Studies in Physics, Degree in progress: Master of Science
2011 – 2012	University of Southampton, United Kingdom Erasmus term in the group of Hendrik Ulbricht

Employment

2010	Diffractive and morphological characterization of nanostructured optical components, Nanogate Advanced Material GmbH
2011	Toolmaking, Phoenix Engineering Gbr
2012	Tutor for “Übung zur Einführung in die Physik I”, Universität Wien
2013	Tutor for “Übung zur Einführung in die Physik II”, Universität Wien
2012 – 2013	Research Assistant in the Group of Markus Aspelmeyer, Universität Wien

Publications

2013	Cavity cooling of an optically levitated nanoparticle, N. Kiesel, F. Blaser, U. Delić, D. Grass, R. Kaltenbaek and M. Aspelmeyer, arXiv: 1304.6679, 2013

Other

2013	Membership for the graduate program CoQus

References

[1] D. Chang, C. Regal, S. Papp, D. Wilson, J. Ye, O. Painter, H. Kimble, and P. Zoller. Cavity opto-mechanics using an optically levitated nanosphere. *Proceedings of the National Academy of Sciences of the United States of America*, 107(3):1005–10, 2010.

[2] O. Romero-Isart, M. Juan, R. Quidant, and J. Cirac. Toward quantum superposition of living organisms. *New Journal of Physics*, 12(3):033015, 2010.

[3] P. Barker and M. N. Shneider. Cavity cooling of an optically trapped nanoparticle. *Physical Review A*, 81(2):023826, 2010.

[4] O. Romero-Isart, A. Pflanzer, M. Juan, R. Quidant, N. Kiesel, M. Aspelmeyer, and J. Cirac. Optically levitating dielectrics in the quantum regime: Theory and protocols. *Physical Review A*, 83(1):013803, 2011.

[5] R. Kaltenbaek, G. Hechenblaikner, N. Kiesel, O. Romero-Isart, Keith C. Schwab, U. Johann, and M. Aspelmeyer. Macroscopic quantum resonators (MAQRO). *Experimental Astronomy*, 34(2):123–164, 2012.

[6] T. Birks, P. Roberts, P. Russell, D. Atkin, and T. Shepherd. Full 2-D photonic bandgaps in silica/air structures. *Electronics Letters*, 31(22):1941–1943, 1995.

[7] P. Russell. Photonic crystal fibers. *Science*, 299(5605):358–62, 2003.

[8] F. Benabid, J. Knight, and P. Russell. Particle levitation and guidance in hollow-core photonic crystal fiber. *Optics Express*, 10(21):1195–203, 2002.

[9] O. Schmidt, M. Garbos, T. Euser, and P. Russell. Metrology of laser-guided particles in air-filled hollow-core photonic crystal fiber. *Optics Letters*, 37(1):91–3, 2012.

[10] Markus Aspelmeyer, Tobias J Kippenberg, and Florian Marquardt. Cavity Optomechanics. *arXiv:1303.0733*, 2013.

[11] N. Kiesel, F. Blaser, U. Delic, D. Grass, R. Kaltenbaek, and M. Aspelmeyer. Cavity cooling of an optically levitated nanoparticle. *arXiv:1304.6679*, 2013.

[12] D. Burnham and D. McGloin. Holographic optical trapping of aerosol droplets. *Optics Express*, 14(9):4176–82, 2006.

[13] M.S. Monteiro, J. Millen, G.A.T. Pender, F. Marquardt, D. Chang, and P.F. Barker. Dynamics of levitated nanospheres: towards the strong coupling regime. *New Journal of Physics*, (15):015001, 2013.

[14] A. Ashkin. Acceleration and trapping of particles by radiation pressure. *Physical Review Letters*, 24(4):156–159, 1970.

[15] A. Ashkin and J. M. Dziedzic. Optical levitation in high vacuum. *Applied Physics Letters*, 28(6):333, 1976.

[16] R. A. Bowling. *Particles on Surfaces 1.* Plenum Press, New York, 1988.

[17] Y. F. Lu, W. D. Song, Y. Zhang, M. H. Hong, and T. C. Chong. Laser removal of particles from solid surfaces. *Riken Review*, 32(32):64–70, 2001.

[18] G. Kumar and S. Beaudoin. Undercut Removal of Micrometer-Scale Particles from Surfaces. *Journal of The Electrochemical Society*, 153(2):G175, 2006.

[19] M. Solanti and A. Goodarz. Particle Removal Mechanisms Under Substrate Acceleration. *The Journal of Adhesion*, 44(3):161–175, 1994.

[20] B. Dahneke. The influence of flattening on the adhesion of particles. *Journal of Colloid and Interface Science*, (40):1–13, 1972.

[21] T. Li. *Fundamental tests of physics with optically trapped microspheres.* PhD thesis, University of Texas, 2011.

[22] Private communication with A. Geraci in 2012.

[23] K. Jousten. *Wutz Handbuch Vakuumtechnik, Theorie und Praxis.* Vieweg und Sohn Verlag, 2004.

[24] Z. Yang and S. V. Garimella. Rarefied gas flow in microtubes at different inlet-outlet pressure ratios. *Physics of Fluids*, 21(5):052005, 2009.

[25] A. Ashkin. Optical Levitation by Radiation Pressure. *Applied Physics Letters*, 19(8):283, 1971.

[26] A. Ashkin. *Optical Trapping and Manipulation of Neutral Particles Using Lasers: A Reprint Volume With Commentaries.* World Scientific Publishing Company, 2006.

[27] Al. Jonás and P. Zemánek. Light at work: the use of optical forces for particle manipulation, sorting, and analysis. *Electrophoresis*, 29(24):4813–51, 2008.

[28] Y. Harada and T. Asakura. Radiation forces on a dielectric sphere in the Rayleigh scattering regime. *Optics Communications*, 124(5-6):529–541, 1996.

[29] S. A. Beresnev, V. G. Chernyak, and G. A. Fomyagin. Motion of a spherical particle in a rarefied gas. Part 2. Drag and thermal polarisation. *Journal of Fluid Mechanics*, 219:405–421, 1990.

[30] T. Li, S. Kheifets, and M. Raizen. Millikelvin cooling of an optically trapped microsphere in vacuum. *Nature Physics*, 7:527–530, 2011.

[31] J. Gieseler, B. Deutsch, R. Quidant, and L. Novotny. Subkelvin Parametric Feedback Cooling of a Laser-Trapped Nanoparticle. *Physical Review Letters*, 109(10):103603, 2012.

[32] D. S. Lemons and A. Gythiel. Paul Langevin's 1908 paper "On the Theory of Brownian Motion" ["Sur la theorie du mouvement brownien," C. R. Acad. Sci. (Paris) 146, 530–533 (1908)]. *American Journal of Physics*, 65(11):1079, 1997.

[33] G. E. Uhlenbeck and L. S. Ornstein. On The Theory Of The Brownian Motion. *Physical Review*, 36(1905):823–841, 1930.

[34] K. Berg-Sørensen and H. Flyvbjerg. Power spectrum analysis for optical tweezers. *Review of Scientific Instruments*, 75(3):594, 2004.

[35] D. Joannopoulos, S. G. Johnson, J. N. Winn, and R. D. Meade. *Photonic Crystals*. Princeton University Press, 2008.

[36] P. Russell. Photonic-Crystal Fibers. *Journal of Lightwave Technology*, 24(12):4729–4749, 2006.

[37] E. Marcatili and R. Schmeltzer. Hollow Metallic and Dielectric Waveguides for Long Distance Optical Transmission and Lasers. *The Bell System Technical Journal*, pages 1783–1809, 1964.

[38] F. Poletti, N. V. Wheeler, M. Petrovich, N. Baddela, E. Numkam Fokoua, J. R. Hayes, D. R. Gray, Z. Li, R. Slavík, and D. J. Richardson. Towards high-capacity fibre-optic communications at the speed of light in vacuum. *Nature Photonics*, 7(4):279–284, 2013.

[39] Michael J. Renn, D. Montgomery, O. Vdovin, and D. Anderson. Laser-guided atoms in hollow-core optical fibers. *Physical Review Letters*, 75(18):3253–3256, 1995.

[40] Michael J. Renn, R. Pastel, and H. Lewandowski. Laser Guidance and Trapping of Mesoscale Particles in Hollow-Core Optical Fibers. *Physical Review Letters*, 82(7):1574–1577, 1999.

[41] R. Omori, T. Kobayashi, and A. Suzuki. Observation of a single-beam gradient-force optical trap for dielectric particles in air. *Optics Letters*, 22(11):816–8, 1997.

[42] M. Garbos, T. Euser, O. Schmidt, S. Unterkofler, and P. Russell. Doppler velocimetry on microparticles trapped and propelled by laser light in liquid-filled photonic crystal fiber. *Optics Letters*, 36(11):2020–2022, 2011.

[43] O. Schmidt, M. Garbos, T. Euser, and P. Russell. Reconfigurable Optothermal Microparticle Trap in Air-Filled Hollow-Core Photonic Crystal Fiber. *Physical Review Letters*, 109(2):024502, 2012.

[44] T. Euser, M. Garbos, J. Chen, and P. Russell. Precise balancing of viscous and radiation forces on a particle in liquid-filled photonic bandgap fiber. *Optics Letters*, 34(23):3674–6, 2009.

[45] V. Shinoj and V. Murukeshan. An integrated hollow-core photonic crystal fiber transverse optical trapping system for optical manipulation and detection. *Journal of Applied Physics*, 111(2):023106, 2012.

[46] V. Shinoj and V. Murukeshan. Hollow-core photonic crystal fiber based multifunctional optical system for trapping, position sensing, and detection of fluorescent particles. *Optics Letters*, 37(10):1607–9, 2012.

[47] V. Shinoj and V. Murukeshan. Numerical investigation and optimisation of hollow-core photonic crystal fibre for optical trapping of fluorescent microparticles. *Micro & Nano Letters*, 6(9):785, 2011.

[48] P. Domachuk, N. Wolchover, M. Cronin-Golomb, and F. G. Omenetto. Effect of hollow-core photonic crystal fiber microstructure on transverse optical trapping. *Applied Physics Letters*, 94(14):141101, 2009.

[49] C. Rajapakse, F. Wang, T. Tang, P. Reece, S. Leon-saval, and A. Argyros. Spectroscopy of 3D-trapped particles inside a hollow-core microstructured optical fiber. *Optics Express*, 20(10):11232–40, 2012.

[50] S. Kuhr, W. Alt, D. Schrader, I. Dotsenko, Y. Miroshnychenko, W. Rosenfeld, M. Khudaverdyan, V. Gomer, A. Rauschenbeutel, and D. Meschede. Coherence Properties and Quantum State Transportation in an Optical Conveyor Belt. *Physical Review Letters*, 91(21):213002, 2003.